CONFIDENTIAL

NASA TECHNICAL MEMORANDUM

UB
NASA TM X-2468

UB
NASA TM X-2468

ANALYSIS OF BASE PRESSURE AND BASE HEATING ON A 5° HALF-ANGLE CONE IN FREE FLIGHT NEAR MACH 20 (REENTRY F)

by James L. Dillon and Howard S. Carter

Langley Research Center
Hampton, Va. 23365

NATIONAL AERONAUTICS AND SPACE ADMINISTRATION • WASHINGTON, D. C. • JANUARY 1972

CONFIDENTIAL

C72 70439

[redacted]

1. Report No.
NASA TM X-2468

2. Government Accession No.

3. Recipient's Catalog No.

4. Title and Subtitle
ANALYSIS OF BASE PRESSURE AND BASE HEATING ON A 5°-HALF-ANGLE CONE IN FREE FLIGHT NEAR MACH 20 (REENTRY F) (U)

5. Report Date
January 1972

6. Performing Organization Code

7. Author(s)
James L. Dillon and Howard S. Carter

8. Performing Organization Report No.
L-8003

9. Performing Organization Name and Address
NASA Langley Research Center
Hampton, Va. 23365

10. Work Unit No.
117-07-04-08

11. Contract or Grant No.

12. Sponsoring Agency Name and Address
National Aeronautics and Space Administration
Washington, D.C. 20546

13. Type of Report and Period Covered
Technical Memorandum

14. Sponsoring Agency Code

15. Supplementary Notes

16. Abstract

Heating and pressure measurements were made on the base of a 396-centimeter-long 5°-half-angle conical spacecraft during reentry at a free-stream Mach number near 20 (Reentry F). The cone surface was beryllium except for the graphite nose which had an initial tip radius of 0.25 centimeter. Angle of attack was less than 1° during the entry from 30.48 kilometers to 15.24 kilometers.

The predicted values of pressure from an extrapolation of Cassanto's turbulent correlation were lower than the measured data except at the lower altitudes. The trend of the laminar heating data and the turbulent data at the highest Reynolds numbers was represented reasonably well by two semiempirical theories. A laminar correlation by King underpredicted the laminar heating data by a factor of 2 to 3.

CLASSIFIED BY IT/DD214(10/3/72)NASC-2431
SUBJECT TO GENERAL DECLASSIFICATION
SCHEDULE OF EXECUTIVE ORDER 11652.
AUTOMATICALLY DOWNGRADED AT
TWO-YEAR INTERVALS.
DECLASSIFIED ON DECEMBER 31, 1978

17. Key Words (Suggested by Author(s))
Base pressure
Base heating
Hypersonic reentry
Slender cone

18. Distribution Statement
[redacted]nt
[redacted]

19. Security Classif. (of this report)
Confidential [redacted]

20. Security Classif. (of this page)
Unclassified

21. No. of Pages
37

22. Price

[redacted]P 4
Downgra[redacted]intervals;
[redacted]classified after 12 years

This material contains information affecting the national defense of the United States within the meaning of the espionage laws, Title 18, U.S.C., Secs. 793 and 794, the transmission or revelation of which in any manner to an unauthorized person is prohibited by law.

[redacted]

[redacted]

ANALYSIS OF BASE PRESSURE AND BASE HEATING ON A 5°-HALF-ANGLE CONE IN FREE FLIGHT NEAR MACH 20 (REENTRY F)*

By James L. Dillon and Howard S. Carter
Langley Research Center

SUMMARY

Heating and pressure measurements were made on the base of a 396-centimeter-long 5°-half-angle conical spacecraft during reentry at a free-stream Mach number near 20 (Reentry F). The cone surface was beryllium except for the graphite nose which had an initial tip radius of 0.25 centimeter. Angle of attack was less than 1° during the entry from 30.48 kilometers to 15.24 kilometers.

The predicted values of pressure from an extrapolation of Cassanto's turbulent correlation were lower than the measured data except at the lower altitudes. The trend of the laminar heating data and the turbulent data at the highest Reynolds numbers was represented reasonably well by two semiempirical theories. A laminar correlation by King underpredicted the laminar heating data by a factor of 2 to 3.

INTRODUCTION

Knowledge of the base-heating and base-pressure levels that a reentry vehicle experiences is of considerable practical importance. The base pressure is an important parameter in the study of near-wake flow-field characteristics. The spacecraft designer may achieve weight reduction by accurately predicting the base heating and base pressure.

Reliable base-pressure and base-heating data are difficult to obtain in wind tunnels primarily because of support-interference effects. Free-flight range testing eliminates the support problem but introduces severe data gathering problems. Hence, full-scale flight data take on more than usual significance where reliable data from other test techniques are lacking. To these authors' knowledge, only a limited amount of base-pressure data and base-heating data from reentry vehicles comparable to the present one are available with which to verify prediction techniques. To help alleviate this scarcity of data, two pressure and four heat-transfer sensors were installed on the base of the Reentry F spacecraft. This vehicle was a 396-centimeter-long 5°-half-angle cone which reentered at a free-stream Mach number near 20. The prime objective of this flight experiment

---

*Title, Unclassified.

[redacted]

was to obtain accurate turbulent heat-transfer and transition data at conditions of simultaneous high Mach number, Reynolds number, total enthalpy, and low ratios of wall temperature to total temperature. Initial results from the experiment are presented in reference 1. The base data obtained during the experiment are presented herein along with semiempirical predictions and previously obtained wind-tunnel and flight data for comparison.

SYMBOLS

C_p	pressure coefficient, $\frac{p - p_\infty}{q_\infty}$
K_{lam}	constant (see eq. (3))
K_{turb}	constant (see eq. (4))
L	spacecraft length, measured from stagnation point along longitudinal axis
M	Mach number
N_{Pr}	Prandtl number
N_{Re}	Reynolds number
N_{St}	Stanton number
p	static pressure
Q	total heat load
q	dynamic pressure
$\dot{q}$	heating rate
R	base radius
r	distance along base radius measured from center of base
s	wetted length of spacecraft

$s' = s + R$

T	temperature
t	time
u	velocity
x	distance from virtual origin measured along longitudinal axis
α	angle of attack
β	angle of sideslip
η	total angle of attack
μ	absolute viscosity
ρ	density
ϕ	circumferential angle (see fig. 2)

Subscripts:

b	local conditions on spacecraft base
c	cone
l	local conditions immediately ahead of spacecraft base
lam	laminar
s	static
ss	local conditions on solid surface that replaces wake
turb	turbulent
w	most windward ray
∞	free-stream conditions

A bar over a symbol indicates an area-weighted average. An asterisk on a symbol denotes reference conditions.

EXPERIMENT

Spacecraft and Launch Vehicle

A photograph of the assembled spacecraft is shown in figure 1. The test vehicle was a 5°-half-angle cone, 396 centimeters long with an initial tip radius of 0.25 centimeter. The primary structure aft of station 21.8 centimeters consisted of a 1.52-centimeter-thick beryllium cone fabricated from seven individual frustums. An ATJ graphite nose tip was mounted forward of 21.8-centimeter station. The graphite nose tip radius was known to increase during reentry, but a definite history of growth could not be established. (See ref. 2.) However, even for the maximum nose radius believed to be possible (ref. 1), the flow conditions at the rear of the cone could accurately be based on sharp-cone concepts. Four VHF and two C-band antenna windows fabricated from slip-cast fused silica were mounted flush with the outer surface in graphite holders on the rearmost conic frustum. The mass of the spacecraft at launch was 272.16 kilograms.

A sketch of the spacecraft is shown in figure 2, and a photograph of the base is shown in figure 3. The center section of the base was closed with a glass phenolic bulkhead and the outer section with a stainless-steel rubber-coated rim cover. The photograph in figure 3 shows the umbilical connectors at the edge of the base, the access hole (closed in this photograph), and the 3.56-centimeter vent hole. The spacecraft support ring was not in place when this photograph was made. The support ring shown in detail A of figure 2 remained with the spacecraft after separation from the third stage of the launch vehicle. Inside the support ring, the base of the spacecraft was flat.

Additional pertinent information concerning design considerations can be found in references 1 and 3. In this paper the primary instrumented ray is designated $\phi = 0^{\circ}$ rather than $\phi = 352.5^{\circ}$ as in reference 3.

The spacecraft was launched with a modified three-stage Scout. The launch vehicle provided the spacecraft with a roll rate of 62 revolutions per minute prior to separation. At an altitude of 60.96 kilometers, the spacecraft had a velocity of 6014 meters per second, and a reentry flight-path angle of -21°. A photograph of the spacecraft—launch-vehicle combination is shown in figure 4. The spacecraft was launched from Wallops Island and reentered near Bermuda where telemetry and tracking stations were located.

Instrumentation

Two pressure orifices were located on the base of the spacecraft as shown in figure 2. Each pressure orifice was 0.152 centimeter in diameter and was connected to

[redacted]

transducers with volumes of 0.065 cc by a 0.43-centimeter inside-diameter tube approximately 22.9 centimeters long. To facilitate accurate pressure measurements at both high and low altitude, the tubing from each orifice was manifolded to enable gages with ranges of 0 to 0.0689 N/cm^2 and 0 to 0.689 N/cm^2 to be installed at each location. The natural frequency of the low- and high-range gages was 2500 Hz and 4500 Hz, respectively. Data from the pressure gages were recorded at 20 samples per second and are believed to be accurate to within ±2 percent of the full-scale reading of the gage. (See ref. 4.)

Four direct-measuring heat gages were also located on the base as shown in figure 2. These gages were the asymptotic type with a range of 0 to 170 W/cm^2. Data from the heat gages were recorded at 10 samples per second and are believed to be accurate to within ±1.14 W/cm^2. (See ref. 4.)

Results and analyses from other instrumentation onboard the spacecraft are reported in references 1, 2, and 5 to 8. These instruments included thermocouples installed in the beryllium wall at 21 locations from which the heating rates, the prime objective of the experiment, were determined; pressure sensors for measurement of surface conical pressure; accelerometers and rate gyros for measurement of body motions; and various diagnostic sensors.

Entry Trajectory and Environment

Meteorological measurements of atmospheric properties were obtained approximately $1\frac{1}{2}$ hours before and after the flight with sonde payloads carried by high-altitude sonde balloons to about 36.58 kilometers and by Arcas rockets to 60.96 kilometers. Ambient temperature and pressure were measured as a function of altitude and were employed in computing free-stream conditions for the flight.

The trajectory and free-stream test conditions for reentry are presented in table I and figure 5. Free-stream dynamic pressure, Mach number, sonic velocity, and Reynolds number were computed by using experimental velocity and measured meteorological data. Total pressure and total enthalpy were computed by use of perfect gas relations. Reference 9 gives detailed explanations and graphical presentations for the complete spaceflight trajectory including locations of receiving stations, radar equipment used, and so forth.

The angle-of-attack component histories that the spacecraft experienced during reentry are presented in figure 6. These histories were determined from onboard measurements of normal and transverse accelerations and pitch, yaw, and roll rates. Reference 7 from which figure 6 was obtained presents the analysis of the spacecraft body motions. During reentry the spacecraft experienced thermal distortion along the longitudinal axis because of differences in temperature on opposite sides of the body. (See

[redacted]

ref. 8.) This distortion was small (less than 0.2°) along the rearward half of the spacecraft and was considered to be negligible in the base data analysis.

DISCUSSION

Basic Data

The base-pressure and base-heating data obtained during the experiment are presented in figures 7 and 8. To correct for small bias errors, the pressure data were shifted to zero at high altitude (≈76.2 km) where the base pressure could be assumed to be negligibly small. The amounts that the pressure data were shifted were as follows:

Location	Data shift, N/cm^2, for gage range of –	
	0 to 0.069 N/cm^2	0 to 0.690 N/cm^2
$r/R = 0$	0	0.0090
$r/R = 0.59$	.0021	.0124

No corrections were necessary for the heating data.

Short-period oscillations, due to angle-of-attack motions of the spacecraft, and data scatter effects are apparent in the measured base-pressure and base-heating data shown in figures 7 and 8. The oscillations associated with variations in instantaneous angle of attack could not be separated from scatter of the data since their magnitudes were similar. The data were, therefore, smoothed as shown in figures 7 and 8. The faired values were used for comparison and correlation. Consequently, the pertinent angle-of-attack conditions are the mean values rather than the instantaneous oscillatory values.

Transition Indications

Thermal data obtained at 12 stations along the primary instrumented ray ($\phi = 0^{\circ}$) were used to determine the movement of transition along the spacecraft. (See ref. 6.) The state of the boundary layer at $x/L = 0.92$ as determined from reference 6 is indicated in figure 9. Although these indications resulted from data obtained along one ray of the spacecraft, data from the opposite ray ($\phi = 180^{\circ}$) indicated similar results. (See ref. 6.)

Also shown in figure 9 is the predicted time at which transition first moved onto the spacecraft from the wake as determined from the base-pressure data by Cassanto's method. (See ref. 10.) According to this method, the onset of transition on the body is determined from the time history of the ratio of pressure measured at the center of the base to free-stream static pressure as shown in figure 9. The minimum point in the curve of p_b/p_∞ as a function of time is determined and the predicted time of transition is assumed to occur at a $\Delta N_{Re,\infty,s}$ of 0.7×10^6 prior to this time. The time of occurrence of transition on the body from this method is shown in figure 9 and is noted to be approximately 1 second (or 2.13 kilometers) later than the first indication of transition at $x/L = 0.92$. (See ref. 6.)

Base Pressure

The ratios of the present base pressures to free-stream static pressures are presented in figure 10 as a function of $N_{Re,\infty,s}$. Also shown in figure 10 are the data from reference 11 which were taken on a 10°-half-angle cone during reentry at $M_\infty = 20$ with measurements made at approximately the same radial locations as those of the present test. Large base-pressure gradients are noted when the boundary layer ahead of the base is laminar; small gradients, for turbulent flow ahead of the base. When correlated as in figure 10, the data are noted to decrease with increasing $N_{Re,\infty,s}$ for laminar flow, to rise slightly with increasing $N_{Re,\infty,s}$ for transitional flow, and, again, to decrease with increasing $N_{Re,\infty,s}$ for turbulent flow. These same trends are noted for the data from reference 11 although the laminar, transitional, and turbulent regimes were not noted in the reference. These trends in the different flow regimes were also mentioned in reference 12 and are shown by the experimental data in reference 13.

Representative pressure distributions for different flow regimes are shown in figure 11. With only two radial data points, some uncertainty exists for the laminar distributions; however, the data from reference 14 show large base-pressure gradients for laminar flow and were used as the basis for fairing the data in the manner shown. Small gradients for turbulent flow are shown in the representative plots.

A comparison of average base pressure for turbulent flow conditions from the present experiment with the turbulent correlation of reference 15 is presented in figure 12. The base-pressure data in this figure are area-weighted averages of the turbulent pressure distributions shown in figure 11. The radial pressure gradients were small for turbulent flow and hence the average values were close to the actual measured values. The average pressures were expressed as ratios to the local static pressure on the cone immediately ahead of the base and are plotted in figure 12 as a function of Mach number at the same location. The parameters p_l and M_l were obtained from sharp-cone theory. The correlation in reference 15 was given for $M_l \leqq 11$, and is extrapolated to the local Mach number conditions of the present experiment. The present data are higher than the extrapolation except at the lower altitudes.

The faired laminar and turbulent base-pressure data are presented in figure 13 in the form $C_{p,b}$ as a function of M_∞ and are compared with data from other sources (refs. 16 to 18). The vacuum-limit curve represents the limiting value for the pressure coefficient, that is, $p_b = 0$. It is noted that base-pressure data from widely different configurations and for a Mach number range from 4 to 20 compare very closely with the vacuum-limit curve when correlated in this manner.

Base Heating

The heating-rate time histories are presented in figure 14 along with the mean total angle of attack and the spacecraft orientation time histories. Note that in the region where the data measured at locations 1, 2, and 4 decrease and then start increasing again ($454.5 < \text{time} < 456.5$) is in the period when the spacecraft changes orientation and the total angle of attack starts to increase.

Representative heating-rate distributions on the base are presented in figure 15 for several altitudes. The fairings shown are through the data from the three gages which were on a line displaced 2.54 centimeters from the $\phi = 270^\circ$ ray. The data from the fourth gage ($\phi = 180^\circ$), indicated by the flagged symbol, were not in agreement with the data from the gage at the same r/R location. According to these distributions, the heating rates were almost constant over the center one-third of the base and decreased over the outer two-thirds.

One unpublished method used by the General Electric Space Systems Division to predict the heating to the base utilizes the following relationships:

$$N_{St,lam} = 0.0513\left(N_{Re,ss,R}\right)^{-0.5} \tag{1}$$

$$N_{St,turb} = 0.0108\left(N_{Re,ss,R}\right)^{-0.3} \tag{2}$$

These empirical relations resulted from data obtained on pointed-cone reentry vehicles with relatively flat bases and low-mass-addition heat-shield materials.

Another approach suggested by AVCO Research and Advanced Development Division for computing base heating is to compute the heating on a solid surface that is assumed to replace the wake by the reference enthalpy method relationships as given in reference 19, and then apply a correction factor to account for separated flow. As determined empirically in reference 20, the correction factors for laminar and turbulent flow ahead of the base should be 0.5 and 1.0, respectively. Thus, the relationships that were used for computing the heating by this method were

$$N_{St,lam} = K_{lam}(0.332)\left(N_{Pr}\right)^{-2/3}\left(N_{Re,ss,s'}\right)^{-1/2}\left(\frac{\rho^*\mu^*}{\rho_{ss}\mu_{ss}}\right)^{1/2} \tag{3}$$

$$N_{St,turb} = K_{turb}(0.185)\left(N_{Pr}\right)^{-2/3}\left(\log_{10} N_{Re,ss,s'}\right)^{-2.58}\left(\frac{\rho^*}{\rho_{ss}}\right)^{0.8}\left(\frac{\mu^*}{\mu_{ss}}\right)^{0.2} \tag{4}$$

where $K_{lam} = 0.5$ and $K_{turb} = 1.0$.

The flight data measured near the center of the base (heating gage 1) are shown in figure 16 and are compared with equations (1) to (4). The experimental data were reduced to the N_{St} form by assuming sharp-cone conditions ahead of the base, expanding isentropically to $p_{ss} = p_b$, and utilizing the resulting ss conditions (that is, u and T). The reduction of the data was based on the pressure measured at the center of the base and on an average measured pressure. As can be seen in figure 16, the theory compares more closely with the data based on the average measured pressure rather than on pressure measured at the center. The laminar correlations (eqs. (1) and (3)) represent the trend of the laminar data reasonably well; equation (1) overpredicts the data by approximately 30 percent and equation (3), by 15 percent. The turbulent correlations (eqs. (2) and (4)) overpredicted by 10 to 20 percent the turbulent data at the highest Reynolds numbers which occurred at the end of the test.

It is noted that the heating data behave in an unusual manner in the region $1.15 \times 10^6 < N_{Re,ss,R} < 5.5 \times 10^6$ $\left(14 \times 10^6 < N_{Re,ss,s'} < 65 \times 10^6\right)$. The expected trend, when the theories and the state of the boundary layer from reference 6 are considered, is denoted by the dashed curve. No explanation can be given for this unusual behavior of the data except to note the following:

(1) The most windward ray of the spacecraft started changing at $t = 454.5$ seconds $\left(N_{Re,ss,R} = 1.15 \times 10^6\right)$ (see fig. 14) which corresponds very closely to the time at which the heating data are noted to fall off after starting to increase from the laminar trend.

(2) Ablation products from the quartz antenna windows were noted to suppress the telemetry signal starting at $t = 455$ seconds and may have affected the base heating.

Another correlation with which the laminar part of the present data can be compared is that of King. (See ref. 21.) In his report, King suggests that the ratio of total heat input to the base to the total heat input to the wall ahead of the base is a function of free-stream Reynolds number. This correlation is presented in figure 17 and can be seen to underpredict the present experimental data by a factor of 2 to 3.

CONCLUSIONS

Flight measurements near Mach 20 of base-pressure and base-heating data on a 5°-half-angle cone 396 centimeters long are presented for reentry down to an altitude of 13.72 kilometers. The data have been compared with semiempirical predictions and the following conclusions are noted:

1. An extrapolation of Cassanto's turbulent base-pressure correlation underpredicted the measured data except at the lower altitudes.

2. The first indication of transition on the body from base pressure was approximately 1 second later than the indication from sidewall data.

3. Two semiempirical relationships predicted the laminar-heating-rate data and the turbulent data at the highest Reynolds numbers at the end of the test reasonably well.

4. A laminar correlation by King underpredicted the laminar heating data by a factor of 2 to 3.

Langley Research Center,
National Aeronautics and Space Administration,
Hampton, Va., December 8, 1971.

[redacted]

REFERENCES

1. Rumsey, Charles B.; Carter, Howard S.; Hastings, Earl C., Jr.; Raper, James L.; and Zoby, Ernest V.: Initial Results From Flight Measurements of Turbulent Heat Transfer and Boundary-Layer Transition at Local Mach Numbers Near 15 (Reentry F). NASA TM X-1856, 1969.
2. Dillon, James L.: Analysis of Surface Pressure on a 5° Cone in Free Flight Near Mach 20 (Reentry F). NASA TM X-2210, 1971.
3. Anon.: Reentry F Turbulent Heat Experiment Familiarization Manual. Doc. No. 67SD7243 (Contract No. NAS 1-6039), Re-Entry Syst. Dep., Gen. Elec. Co., Oct. 30, 1967. (Available as NASA CR-66501.)
4. Carter, Howard S.; Raper, James L.; Hinson, William F.; and Morris, W. Douglas: Basic Measurements From a Turbulent-Heating Flight Experiment on a 5° Half-Angle Cone at Mach 20 (Reentry F). NASA TM X-2308, 1971
5. Howard, Floyd G.: Thermal Analysis Methods and Basic Heat-Transfer Data for a Turbulent Heating Flight Experiment at Mach 20 (Reentry F). NASA TM X-2282, 1971.
6. Wright, Robert L.; and Zoby, Ernest V.: Flight Measurements of Boundary-Layer Transition on a 5° Half-Angle Cone at a Free-Stream Mach Number of 20 (Reentry F). NASA TM X-2253, 1971.
7. Woodbury, Gerard E.; and Morris, W. Douglas: Angle-of-Attack Analysis of a Spinning Slender Cone With Slight Aerodynamic and Mass Asymmetries. NASA TN D-5948, 1970.
8. Alley, Vernon L., Jr.; and Guillotte, Robert J.: Postflight Analysis of Thermal Distortions of the Reentry F Spacecraft. NASA TM X-2250, 1971.
9. Jennings, K. F.: Scout S-164C. Final Flight Report. Rep. No. 3-32000/8R-141 (Contract No. NAS 1-6020), LTV Missiles and Space Division, July 30, 1968.
10. Cassanto, J. M.: A Method of Determining Onset of Boundary Layer Transition From Flight Test Base Pressure Data. ATFM 67-23, Gen. Elec. Co., Oct. 16, 1967.
11. King, Hartley H.: A Correlation of Re-Entry and Laboratory Base Flow Data. EOS Res. Note No. 29 (Contract AF 04(694)-570), Electro-Optical Systems, Inc., Nov. 1965.
12. Kavanau, L. L.: Base Pressure Studies in Rarefied Supersonic Flows. J. Aeron. Sci., vol. 23, no. 3, Mar. 1956, pp. 193-207, 230.
13. Cassanto, John M.: Base Pressure Results at M = 4 Using Free-Flight and Sting-Supported Models. AIAA J., vol. 6, no. 7, July 1968, pp. 1411-1414.

[redacted]

14. Cassanto, John M.: Radial Base-Pressure Gradients in Laminar Flow. AIAA J. (Tech. Notes), vol. 5, no. 12, Dec. 1967, pp. 2278-2279.

15. Cassanto, John M.: Effect of Cone Angle and Bluntness Ratio on Base Pressure. AIAA J., vol. 3, no. 12, Dec. 1965, pp. 2351-2352. (Title corrected per erratum, AIAA J., vol. 4, no. 2, Feb. 1966, p. 384.)

16. Saltzman, Edwin J.: Base Pressure Coefficients Obtained From the X-15 Airplane for Mach Numbers Up to 6. NASA TN D-2420, 1964.

17. Zarin, Neil A.: Base Pressure Measurements on Sharp and Blunt 9° Cones at Mach Numbers From 3.50 to 9.20. AIAA J., vol. 4, no. 4, Apr. 1966, pp. 743-745.

18. Love, Eugene S.: Base Pressure at Supersonic Speeds on Two-Dimensional Airfoils and on Bodies of Revolution With and Without Fins Having Turbulent Boundary Layers. NACA TN 3819, 1957. (Supersedes NACA RM L53C02.)

19. Schurmann, E. E. H.: Engineering Methods for the Analysis of Aerodynamic Heating. RAD-TM-63-68 (Contract AF 04(694)-312), AVCO Corp., Nov. 11, 1963.

20. Anon.: Aerodynamic Heat Transfer Handbook – Vol. I. Doc. No. D2-9514, Boeing Airplane Co., 1961.

21. King, Hartley H.: An Analysis of Base Heat Transfer in Laminar Flow. EOS Res. Note No. 14 (Contract DA-04-495-AMC-28-(Z)), Electro-Optical Systems, Inc., Sept. 1963.

[redacted]

TABLE I.- TRAJECTORY AND FREE-STREAM CONDITIONS

Time, sec	Altitude, m	Velocity, m/sec	Mach number	Reynolds number per meter	Dynamic pressure, N/m^2	Sonic velocity, m/sec	Static pressure, N/m^2	Static enthalpy, J/kg	Total enthalpy, J/kg	Static temperature, °K	Static density, kg/m^3	Dynamic viscosity, N-sec/m^2	Total pressure, N/m^2
439.38	61000	6013.0	19.13	106393	5034.76	314.31	20.08	246069	18266630	245.0	.00027850	.000015739	70652867
439.61	60500	6013.6	19.08	113519	5394.59	315.10	21.51	247317	18271728	246.2	.00029834	.000015804	74446882
439.84	60000	6014.3	19.03	120589	5754.54	315.90	22.95	248565	18276726	247.5	.00031818	.000015869	78101010
440.07	59500	6014.9	18.99	128694	6166.86	316.69	24.56	249813	18281725	248.7	.00034090	.000015933	82229822
440.30	59000	6015.5	18.94	137085	6596.10	317.48	26.24	251061	18286724	250.0	.00036456	.000015997	86401359
440.52	58500	6016.1	18.90	146428	7074.61	318.27	28.04	252309	18291723	251.2	.00039092	.000016061	90839080
440.75	58000	6016.8	18.85	155830	7559.59	319.05	30.02	253557	18296722	252.5	.00041763	.000016125	95667990
440.98	57500	6017.4	18.81	164898	8031.97	319.84	32.13	254805	18301722	253.7	.00044364	.000016189	100738320
441.21	57000	6018.0	18.76	173899	8504.54	320.62	34.24	256053	18306723	254.9	.00046964	.000016252	105629487
441.44	56500	6018.6	18.72	184984	9082.91	321.40	36.60	257301	18311723	256.2	.00050148	.000016316	111123458
441.67	56000	6019.3	18.68	197190	9720.81	322.18	39.11	258549	18316724	257.4	.00053659	.000016379	116854008
~~441.89~~	~~55500~~	~~6019.9~~	~~18.63~~	~~209306~~	~~10358.98~~	~~322.95~~	~~41.62~~	259797	18321726	~~258.7~~	.00057170	.000016442	122384921
442.12	55000	6020.5	18.59	220688	10965.28	323.73	44.55	261044	18326728	259.9	.00060503	.000016505	128946228
442.35	54500	6021.2	18.55	231873	11566.12	324.50	47.55	262292	18331730	261.2	.00063805	.000016568	135496417
442.58	54000	6021.7	18.51	244603	12248.44	325.27	50.70	263540	18336276	262.4	.00067557	.000016631	142193206
442.81	53500	6022.2	18.47	258951	13016.87	326.04	53.98	264788	18340699	263.6	.00071783	.000016694	149054016
443.03	53000	6022.8	18.42	272911	13771.20	326.81	57.64	266036	18345122	264.9	.00075929	.000016756	156679791
443.26	52500	6023.3	18.38	286695	14521.81	327.58	61.39	267284	18349545	266.1	.00080054	.000016818	164319236
443.49	52000	6023.8	18.34	302301	15370.29	328.34	65.36	268532	18353969	267.4	.00084716	.000016881	172253829
443.72	51500	6024.3	18.30	321608	16413.51	329.10	69.75	269780	18358393	268.6	.00090450	.000016943	181008073
443.94	51000	6024.9	18.26	340780	17457.10	329.86	74.14	271028	18362817	269.9	.00096184	.000017005	189469049
444.17	50500	6025.4	18.25	360752	18498.61	330.05	78.80	271339	18366305	270.2	.00101905	.000017020	200720425
444.40	50000	6025.9	18.25	380885	19537.37	330.10	83.83	271422	18369564	270.2	.00107608	.000017024	213423479
444.63	49500	6026.5	18.25	407182	20893.09	330.15	89.41	271504	18372824	270.3	.00115055	.000017028	227537049
444.85	49000	6027.0	18.25	433684	22260.27	330.20	95.01	271587	18376083	270.4	.00122563	.000017032	241687492
445.08	48500	6027.4	18.25	460267	23632.16	330.25	100.88	271669	18378872	270.5	.00130097	.000017036	256472384
445.31	48000	6027.9	18.24	488431	25085.99	330.30	107.54	271751	18381537	270.6	.00138080	.000017040	273265017
445.53	47500	6028.3	18.24	518918	26660.12	330.35	114.47	271834	18384202	270.7	.00146724	.000017045	290697475
445.76	47000	6028.7	18.24	552736	28406.38	330.40	121.54	271916	18386867	270.7	.00156312	.000017049	308476996
445.99	46500	6029.1	18.24	589904	30325.76	330.45	129.39	271998	18389339	270.8	.00166852	.000017053	328226904
446.21	46000	6029.5	18.24	629712	32381.78	330.50	137.73	272081	18391499	270.9	.00178144	.000017057	349139073
446.44	45500	6029.8	18.24	675103	34726.25	330.55	146.63	272163	18393659	271.0	.00191020	.000017061	371457752
446.67	45000	6030.2	18.23	717486	36917.31	330.60	156.32	272245	18395819	271.1	.00203049	.000017065	395757711
446.89	44500	6030.5	18.27	763797	39187.95	329.99	166.28	271242	18396893	270.1	.00215513	.000017015	426534968
447.12	44000	6030.8	18.33	826252	42184.57	328.96	177.06	269548	18396679	268.4	.00231974	.000016931	464251059
447.34	43500	6031.0	18.39	884730	44946.95	327.92	188.64	267853	18396443	266.7	.00247145	.000016847	505621220
447.57	43000	6031.2	18.45	944693	47754.19	326.89	200.80	266159	18396206	265.0	.00262559	.000016762	550259242
447.80	42500	6031.5	18.51	1018386	51220.90	325.84	214.24	264465	18395970	263.3	.00281597	.000016677	600337757
448.02	42000	6031.6	18.57	1105171	55303.67	324.80	228.18	262770	18395238	261.6	.00304027	.000016592	653862419
448.25	41500	6031.7	18.63	1194202	59452.34	323.75	243.49	261076	18394081	259.9	.00326824	.000016507	713555687
448.47	41000	6031.8	18.69	1289751	63877.15	322.70	260.05	259382	18392925	258.3	.00351138	.000016421	779457201
448.70	40500	6031.9	18.75	1396305	68793.79	321.64	277.62	257687	18391768	256.6	.00378154	.000016335	851245593
448.92	40000	6032.0	18.81	1507630	73887.87	320.58	296.58	255993	18390498	254.9	.00406146	.000016249	930412435
449.15	39500	6031.9	18.87	1610478	78507.62	319.52	316.66	254299	18388287	253.2	.00431553	.000016163	1016325481
~~449.38~~	~~39000~~	~~6031.8~~	18.94	1732518	84002.81	318.45	~~337.91~~	252605	18386077	251.5	.00461772	.000016076	1109722261
449.60	38500	6031.7	19.00	1862983	89838.86	317.38	361.32	250910	18383866	249.8	.00493868	.000015989	1214397098
449.83	38000	6031.6	19.06	2031800	97444.06	316.31	386.84	249216	18381655	248.1	.00535691	.000015902	1330796410
450.05	37500	6031.4	19.13	2204565	105143.53	315.23	412.91	247522	18378332	246.4	.00578070	.000015815	1453867029
450.28	37000	6031.0	19.19	2408863	114243.03	314.15	442.53	245827	18374464	244.8	.00628174	.000015727	1594930487

[redacted]

TABLE I.- TRAJECTORY AND FREE-STREAM CONDITIONS – Concluded

Time, sec	Altitude, m	Velocity, m/sec	Mach number	Reynolds number per meter	Dynamic pressure, N/m^2	Sonic velocity, m/sec	Static pressure, N/m^2	Static enthalpy, J/kg	Total enthalpy, J/kg	Static temperature, °K	Static density, kg/m^3	Dynamic viscosity, $N\text{-}sec/m^2$	Total pressure, N/m^2
450.50	36500	6030.6	19.26	2629386	123996.30	313.07	473.50	244133	18370595	243.1	.00681885	.000015639	1747065023
450.73	36000	6030.3	19.32	2856731	133948.87	311.98	508.21	242439	18366727	241.4	.00736705	.000015551	1919970345
450.95	35500	6029.8	19.39	3095930	144327.16	310.89	545.84	240744	18362346	239.7	.00793902	.000015462	2111615874
451.18	35000	6029.1	19.46	3360388	155736.69	309.79	585.01	239050	18356243	238.0	.00856871	.000015373	2317097986
451.40	34500	6028.4	19.52	3669036	169034.48	308.69	628.33	237356	18350140	236.3	.00930263	.000015284	2548444931
451.63	34000	6027.6	19.58	3979865	182459.52	307.79	675.96	235977	18344352	235.0	.01004390	.000015211	2795007835
451.85	33500	6026.9	19.60	4295289	196520.71	307.44	726.58	235428	18339396	234.4	.01082057	.000015182	3026073206
452.08	33000	6025.9	19.62	4629531	211372.61	307.08	780.38	234878	18332809	233.9	.01164221	.000015153	3272666269
452.30	32500	6024.8	19.64	5000253	227819.85	306.72	839.21	234329	18325773	233.3	.01255260	.000015124	3543585465
452.53	32000	6023.6	19.66	5392455	245165.57	306.36	901.58	233780	18317735	232.8	.01351393	.000015095	3832422286
452.75	31500	6022.2	19.68	5846084	265215.76	306.00	970.55	233231	18308909	232.2	.01462582	.000015066	4152670905
452.98	31000	6020.7	19.72	6349884	286725.18	305.17	1044.21	231978	18298510	231.0	.01582000	.000014999	4543825987
453.20	30500	6018.9	19.78	6891615	309499.65	304.23	1123.68	230537	18286199	229.5	.01708686	.000014922	4985702528
453.42	30000	6017.0	19.83	7451171	332797.23	303.27	1210.15	229096	18273439	228.1	.01838460	.000014845	5475151313
453.65	29500	6014.5	19.89	8097089	359615.54	302.32	1302.14	227654	18257066	226.7	.01988257	.000014768	6004078746
453.87	29000	6012.0	19.94	8889573	392534.37	301.36	1403.76	226213	18240699	225.2	.02172058	.000014691	6597386907
454.10	28500	6008.7	20.00	9792079	429911.89	300.40	1514.00	224772	18219481	223.8	.02381498	.000014613	7246871570
454.32	28000	6005.3	20.05	10673486	465847.03	299.43	1633.70	223330	18197656	222.4	.02583487	.000014535	7964394282
454.55	27500	6001.2	20.07	11486928	499550.98	298.91	1765.36	222547	18172724	221.6	.02774129	.000014493	8671025566
454.77	27000	5996.9	20.06	12376440	537740.52	298.87	1905.18	222496	18146630	221.5	.02990544	.000014490	9318374951
455.00	26500	5992.0	20.05	13349108	579420.80	298.84	2056.25	222444	18117584	221.5	.03227562	.000014487	10009159186
455.23	26000	5986.6	20.03	14464276	627129.93	298.80	2219.31	222393	18084818	221.4	.03499715	.000014484	10743353914
455.45	25500	5980.8	20.01	15611874	676103.44	298.77	2395.24	222341	18050331	221.4	.03780301	.000014482	11527137134
455.68	25000	5974.0	19.99	16873415	729766.18	298.73	2587.63	222290	18009799	221.3	.04089632	.000014479	12365432512
455.90	24500	5967.2	19.97	18207499	786415.74	298.70	2793.79	222238	17969239	221.3	.04417157	.000014476	13256380507
456.13	24000	5958.9	19.95	19619617	846064.24	298.66	3017.97	222187	17919784	221.2	.04765458	.000014473	14194144759
456.35	23500	5950.6	19.92	21122500	909427.67	298.63	3256.76	222135	17870399	221.2	.05136672	.000014470	15182280799
456.58	23000	5940.8	19.89	22768793	978518.23	298.60	3513.78	222084	17812728	221.1	.05545016	.000014468	16209332840
456.81	22500	5930.8	19.90	24706948	1056283.74	297.96	3798.09	221147	17752149	220.2	.06006058	.000014417	17571255095
457.03	22000	5919.4	19.92	26999375	1146500.98	297.10	4102.55	219866	17683565	218.9	.06544159	.000014347	19109093400
457.26	21500	5907.1	19.94	29363771	1238249.51	296.23	4434.96	218585	17609792	217.6	.07097315	.000014277	20778038163
457.49	21000	5893.8	19.95	31848056	1333411.28	295.36	4790.06	217303	17530343	216.4	.07677263	.000014207	22548506213
457.72	20500	5879.0	19.96	34807859	1446482.94	294.49	5183.84	216022	17442198	215.1	.08370282	.000014137	24476794650
457.95	20000	5863.5	19.96	37868627	1561720.28	293.62	5607.79	214741	17350472	213.8	.09084819	.000014066	26541253538
458.18	19500	5845.6	19.96	41552601	1699833.97	292.74	6067.52	213460	17244578	212.5	.09948990	.000013996	28703268417
458.41	19000	5827.6	19.96	45308461	1838411.43	291.86	6574.80	212179	17138325	211.3	.10826804	.000013925	31085555067
458.64	18500	5806.0	19.95	49300696	1982840.75	290.98	7125.95	210898	17012062	210.0	.11764246	.000013854	33533974056
458.87	18000	5784.4	19.93	54234468	2162013.56	290.09	7728.05	209616	16886262	208.7	.12923060	.000013783	36198684913
459.10	17500	5759.1	19.91	59186593	2336929.26	289.20	8381.11	208335	16739168	207.4	.14091801	.000013711	38899509033
459.34	17000	5733.2	19.83	63942069	2510026.42	288.98	9099.62	208011	16590451	207.1	.15272684	.000013693	41159125309
459.57	16500	5704.2	19.73	68714693	2683752.39	288.98	9865.69	208011	16425404	207.1	.16495940	.000013693	43089647519
459.81	16000	5674.1	19.47	72038991	2838850.38	291.42	10725.21	211541	16258229	210.6	.17634890	.000013890	42611149990
460.04	15500	5641.3	19.21	75850328	3008722.50	293.57	11589.91	214671	16076073	213.7	.18908464	.000014062	42047373901
460.28	15000	5606.6	19.19	82676157	3231942.48	292.10	12550.74	212530	15879571	211.6	.20563277	.000013944	45172937291
460.52	14500	5569.3	19.03	88126395	3432547.29	292.63	13603.83	213303	15672409	212.4	.22133385	.000013987	46173113573
460.76	14000	5529.3	18.76	92906667	3634692.49	294.66	14727.92	216268	15454308	215.3	.23776845	.000014150	45350738906
461.01	13500	5486.9	18.49	97140544	3814434.94	296.67	15922.33	219233	15224531	218.3	.25339688	.000014312	44359033738
461.25	13000	5441.3	18.27	104067490	4078555.61	297.82	17204.94	220925	14977811	220.0	.27550364	.000014405	44066946856
461.50	12500	5393.2	18.23	113347541	4352639.22	295.77	18605.06	217905	14715036	217.0	.29928590	.000014240	47000961082
461.74	12000	5341.2	18.18	123673700	4648621.81	293.72	20116.93	214885	14433604	213.9	.32589630	.000014074	49876711121

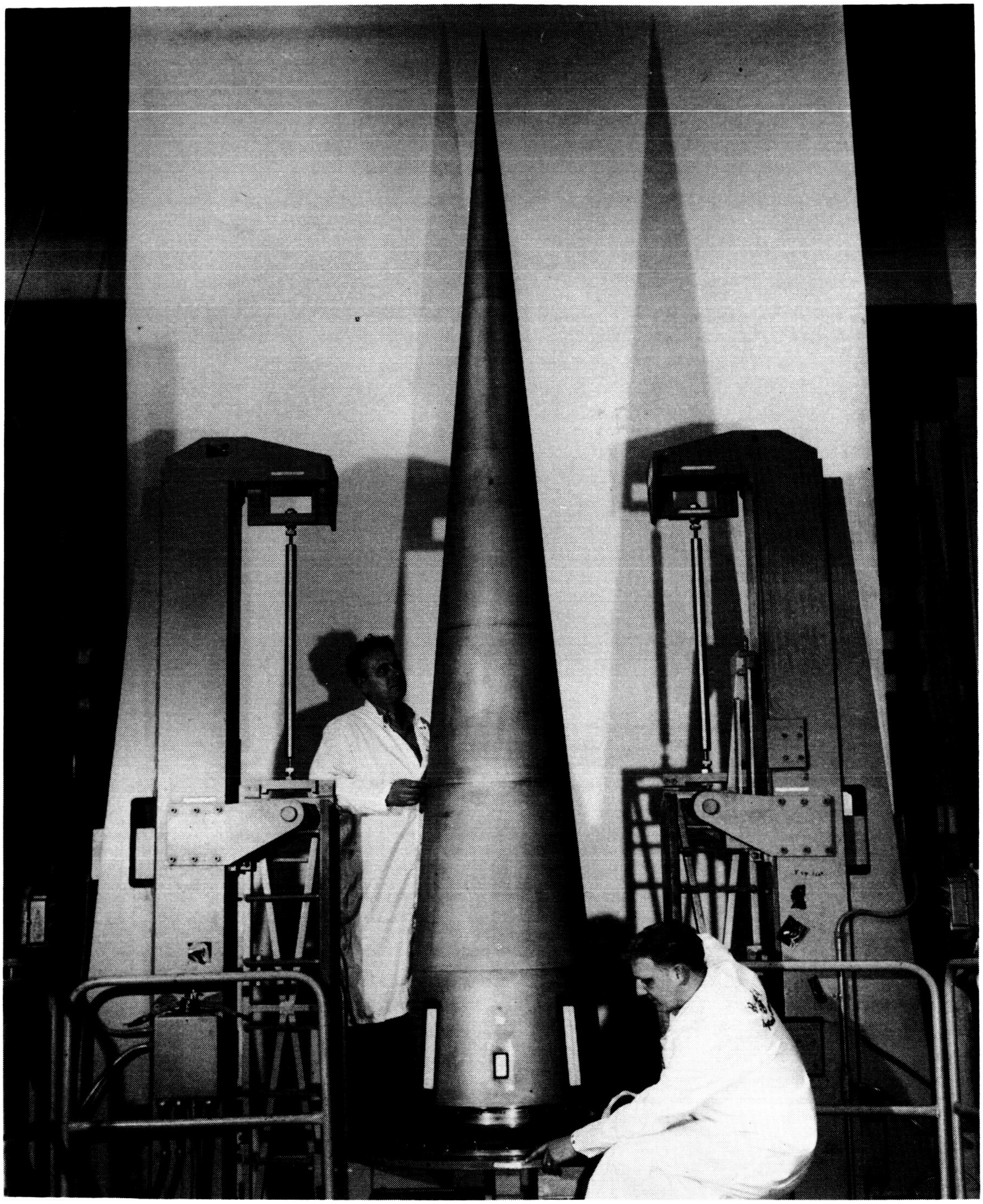

L-68-203.1

Figure 1.- Photograph of spacecraft.

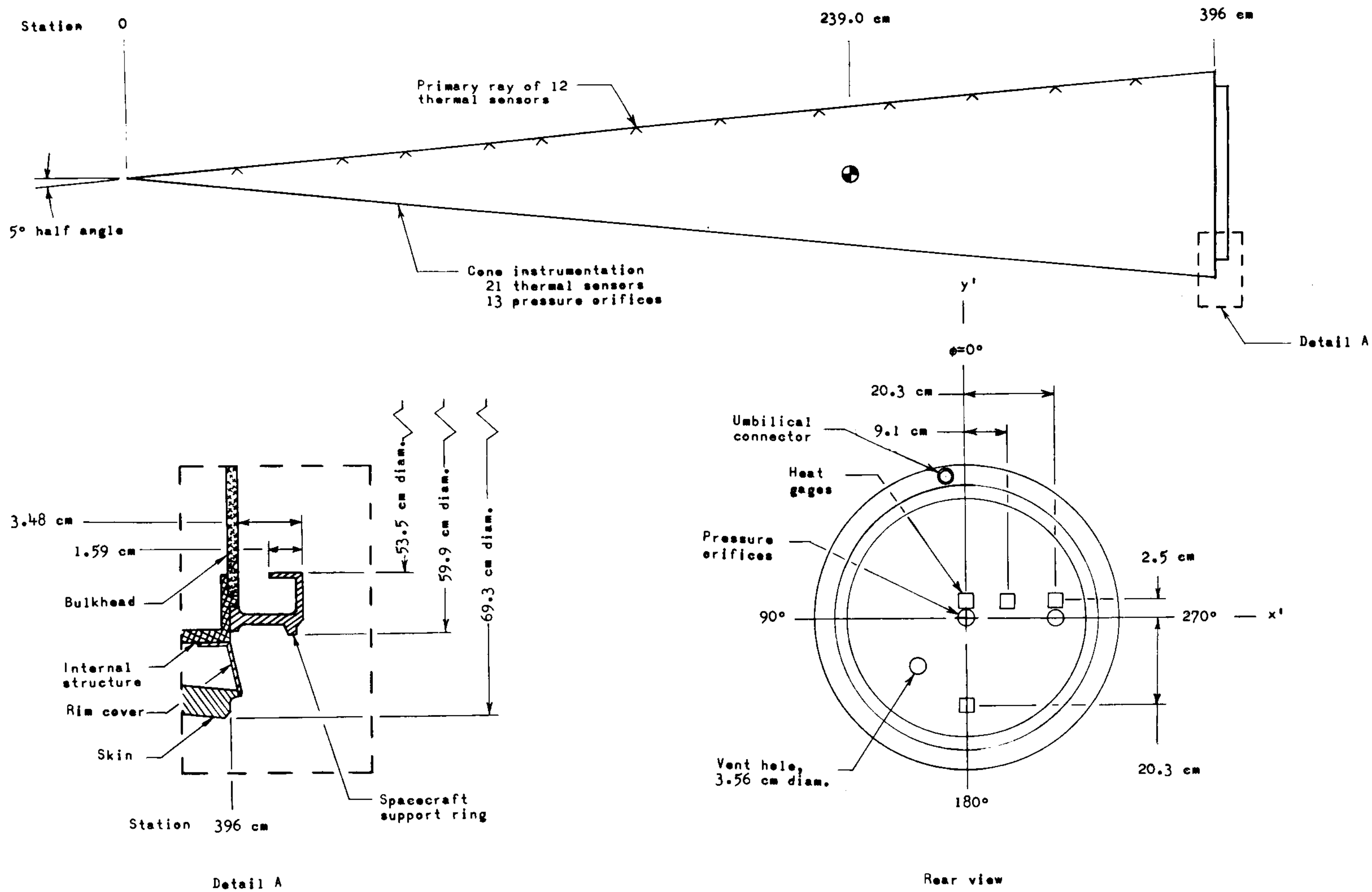

Figure 2.- Sketch of spacecraft showing base configuration and instrumentation.

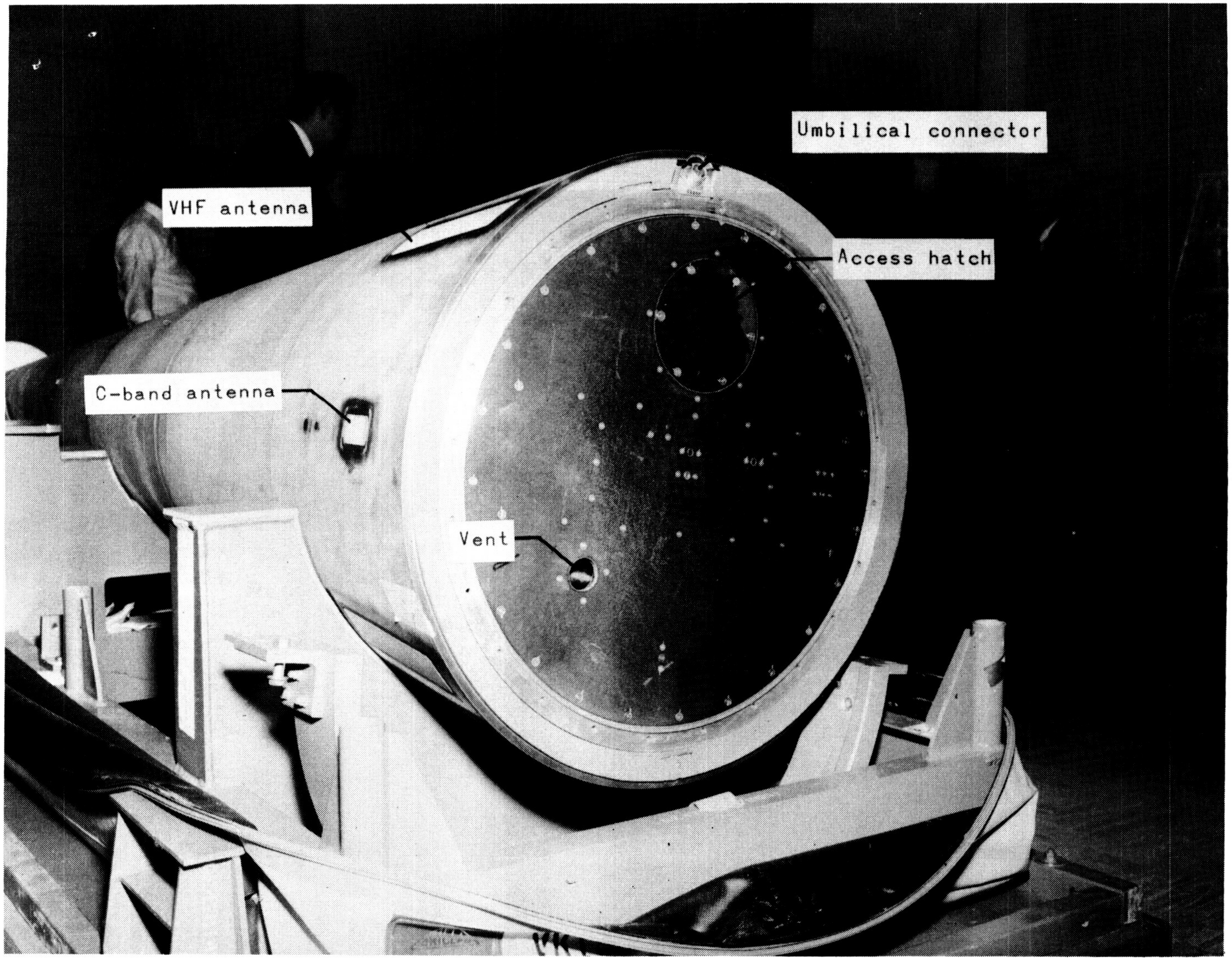

L-71-7142

Figure 3.- Photograph of spacecraft base.

[redacted]

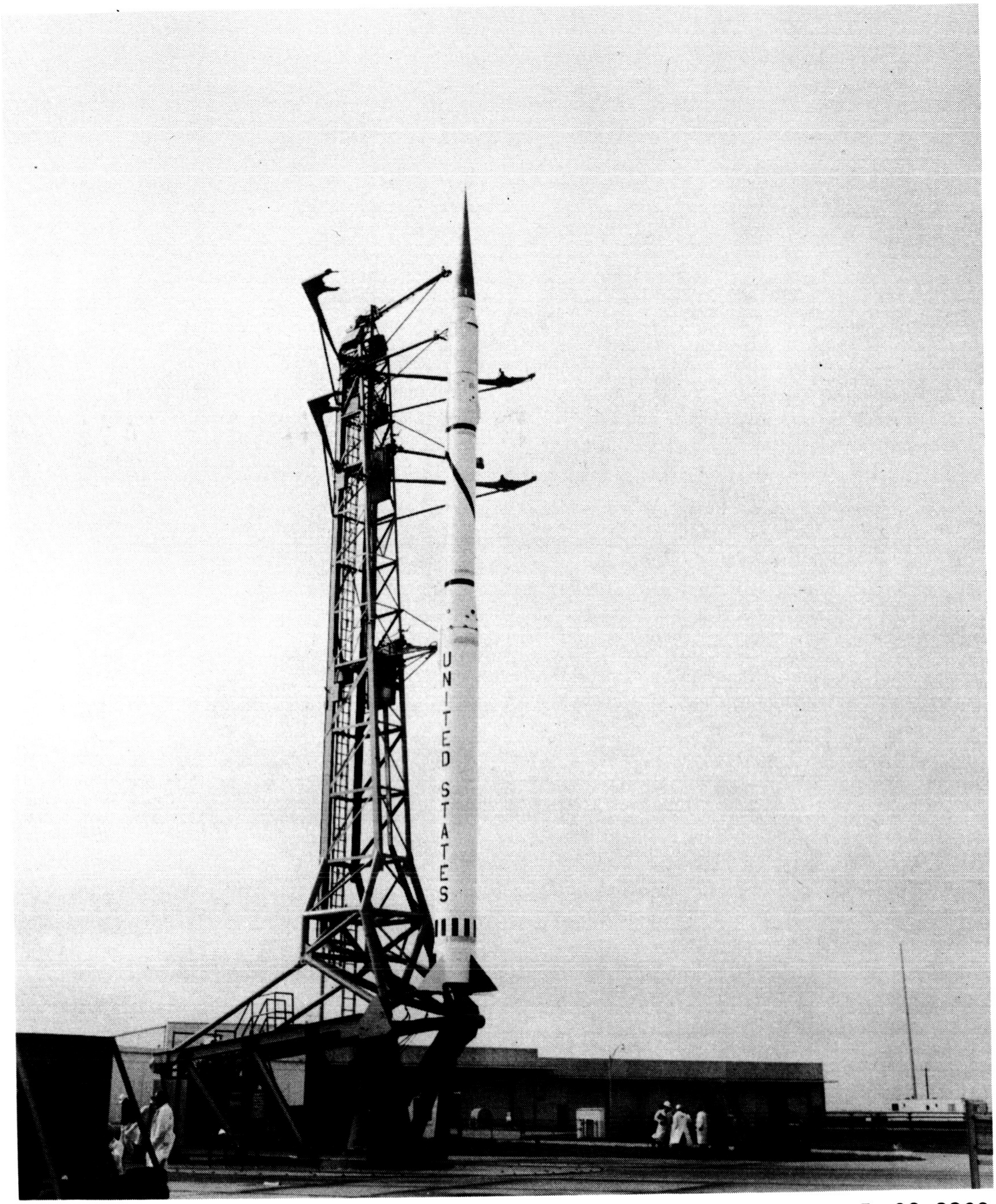

L-68-2263

Figure 4.- Photograph of spacecraft and launch vehicle on launcher.

[redacted]

[redacted]

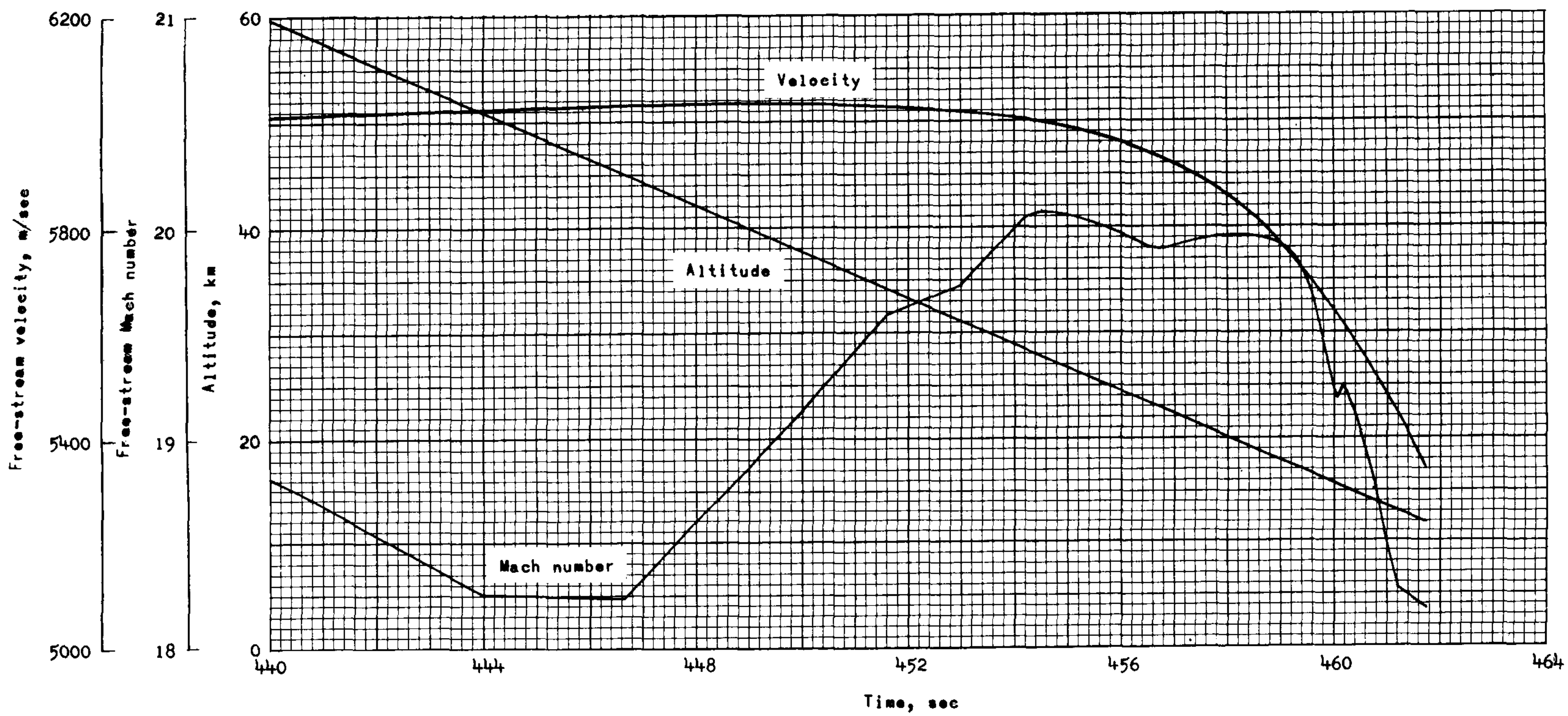

Figure 5.- History of free-stream Mach number, altitude, and velocity.

[redacted]

[redacted]

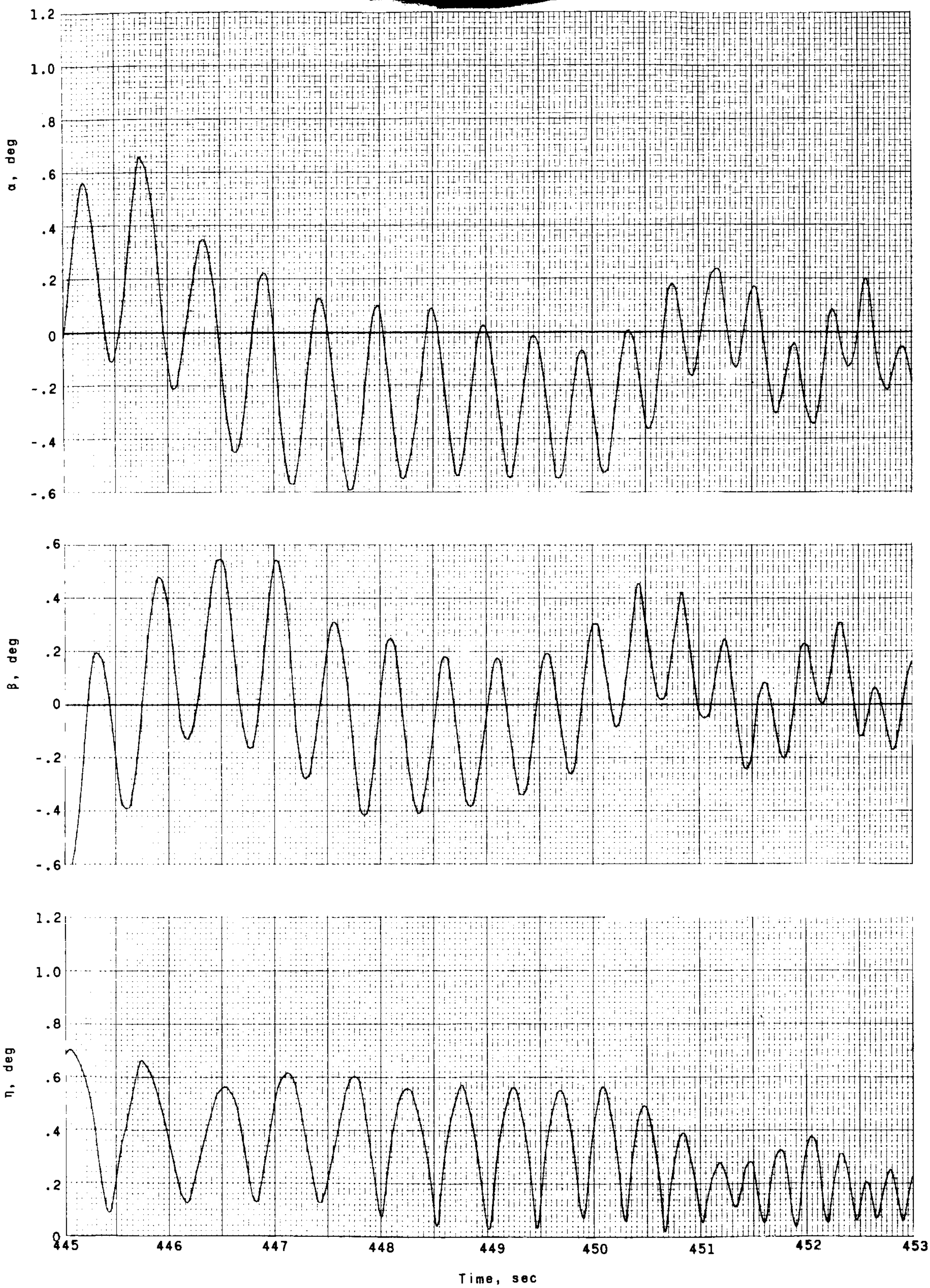

(a) Time, 445 to 453 seconds.

Figure 6.- Angle of attack, angle of sideslip, and total angle of attack as a function of time.

[redacted]

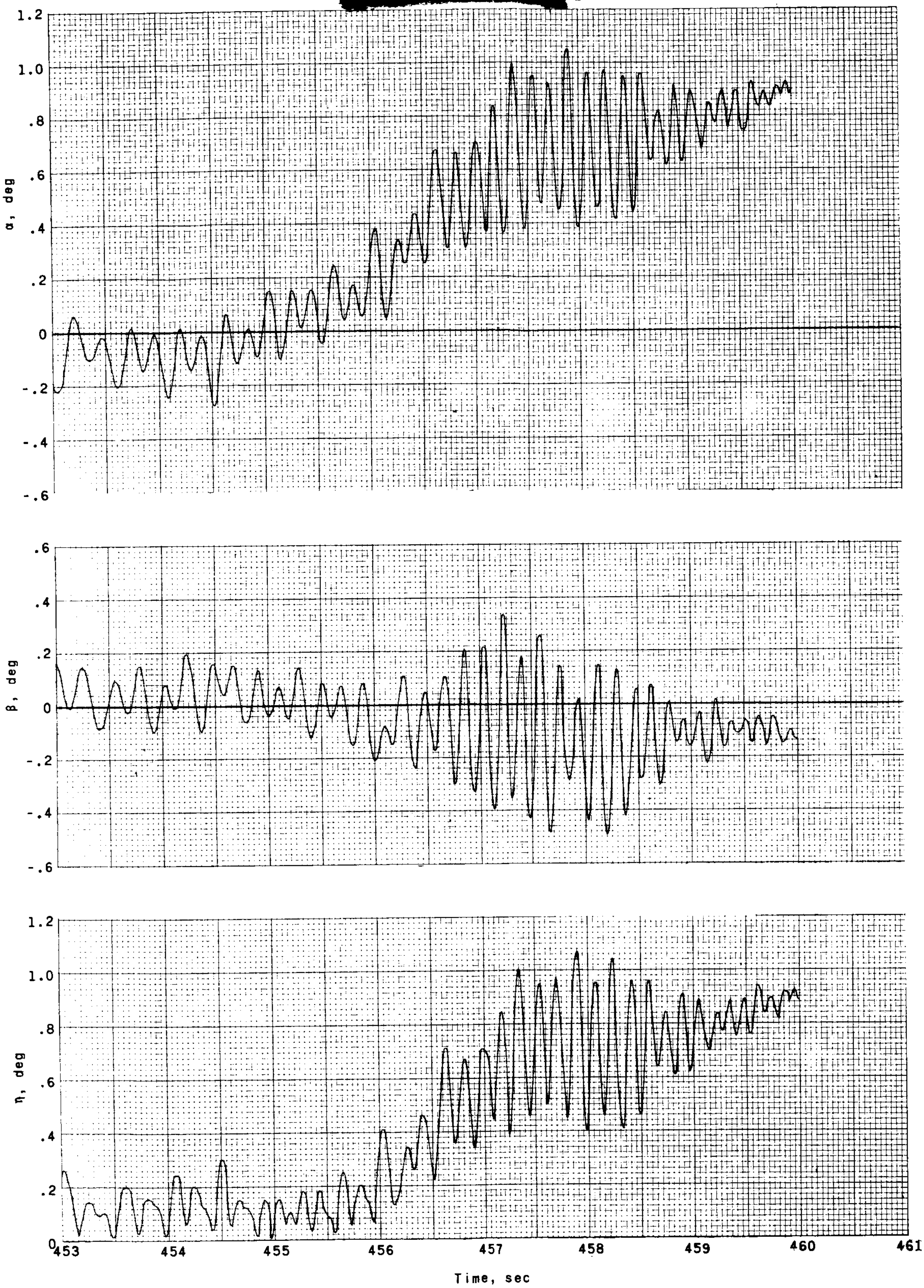

(b) Time, 453 to 461 seconds.

Figure 6.- Concluded.

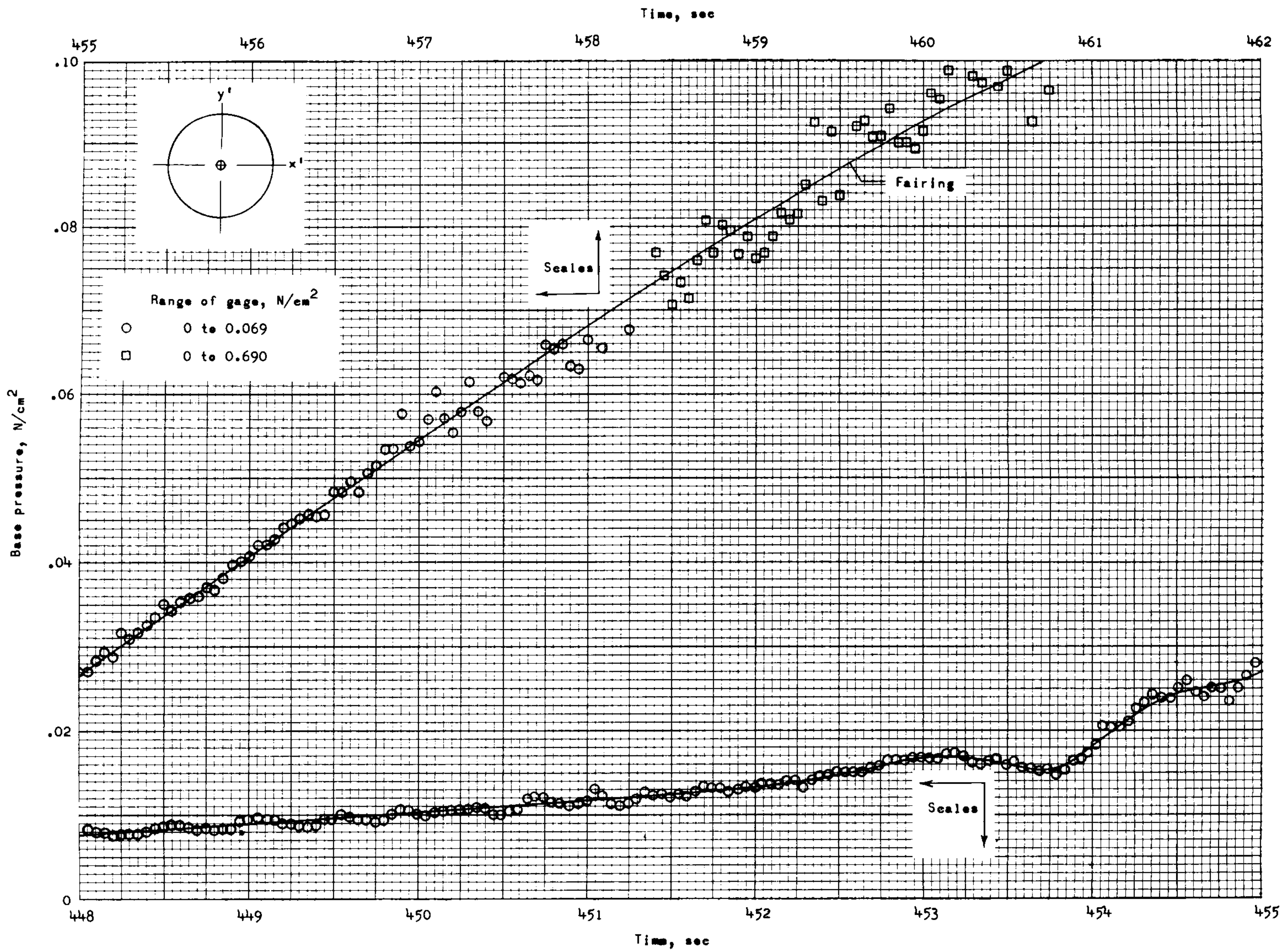

(a) For orifice at center.

Figure 7.- Base-pressure history during reentry.

[redacted]

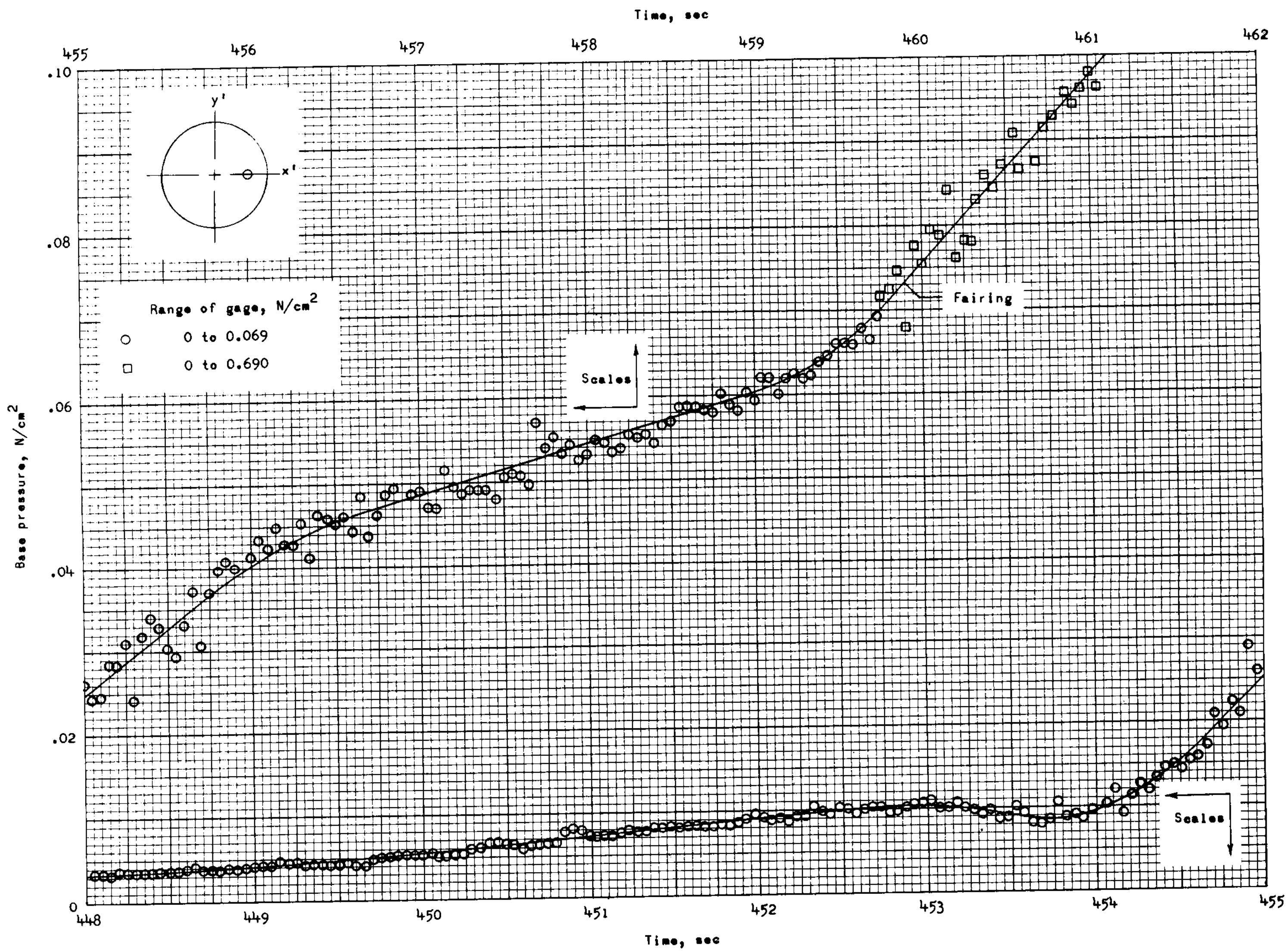

(b) For x' = 0 centimeter; y' = 20 centimeters.

Figure 7.- Concluded.

[redacted]

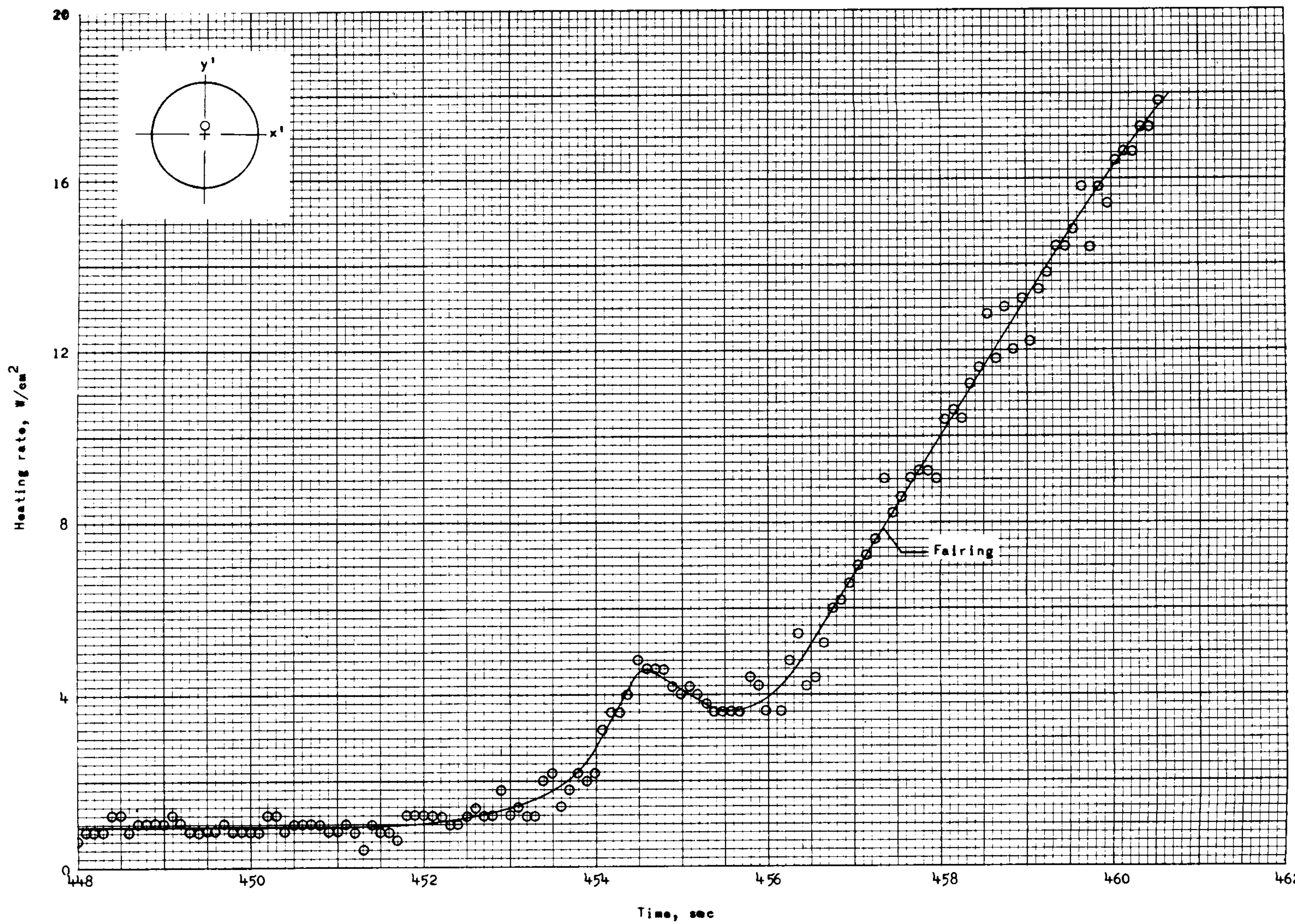

(a) For x' = 0 centimeter; y' = 2.54 centimeters.

Figure 8.- Heating-rate histories during reentry for the four measurement stations on the base.

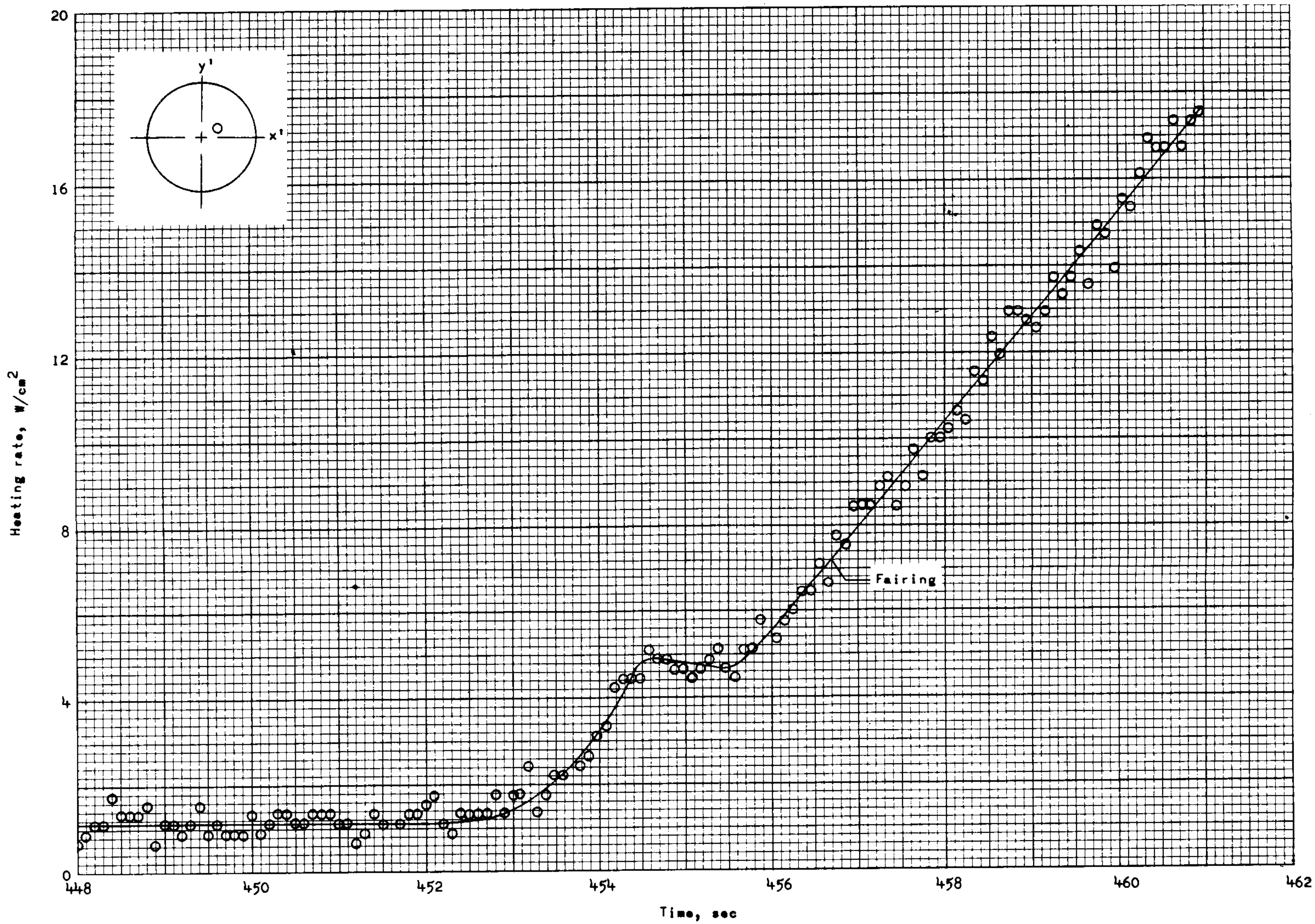

(b) For x' = 9.14 centimeters; y' = 2.54 centimeters.

Figure 8.- Continued.

[redacted]

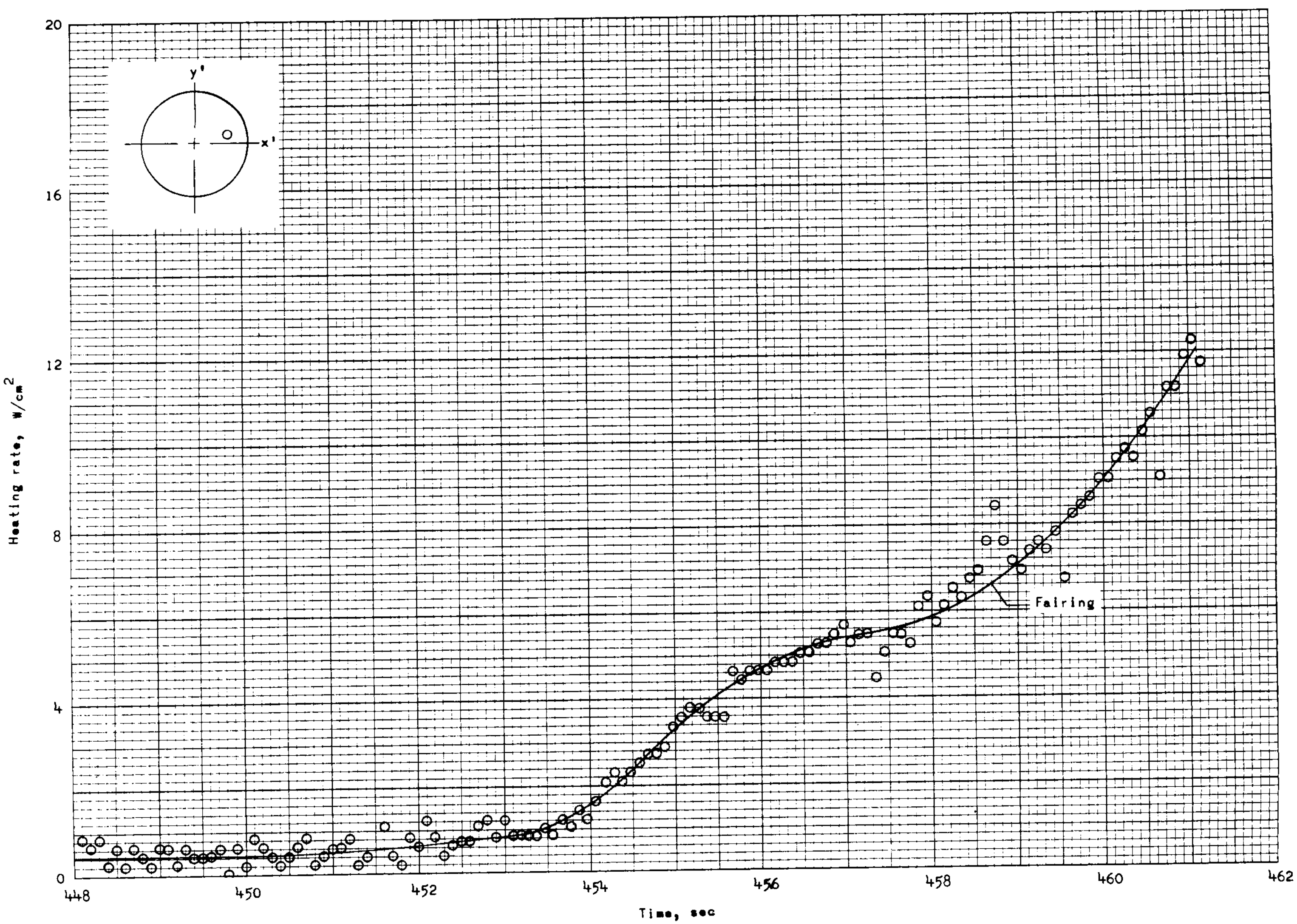

(c) For $x' = 20.32$ centimeters; $y' = 2.54$ centimeters.

Figure 8.- Continued.

[redacted]

[redacted]

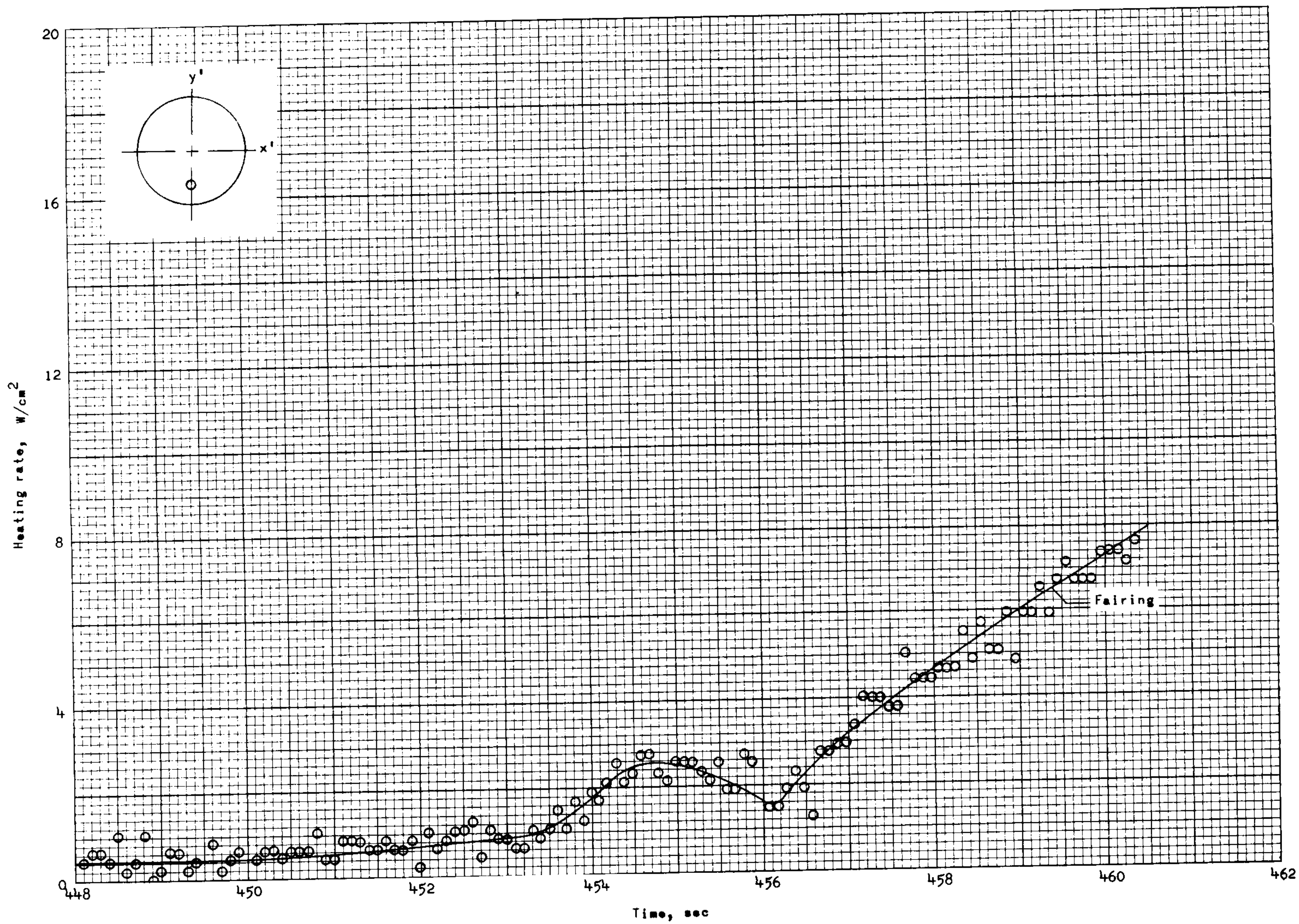

(d) For x' = 0 centimeter; y' = -20.32 centimeters.

Figure 8.- Concluded.

[redacted]

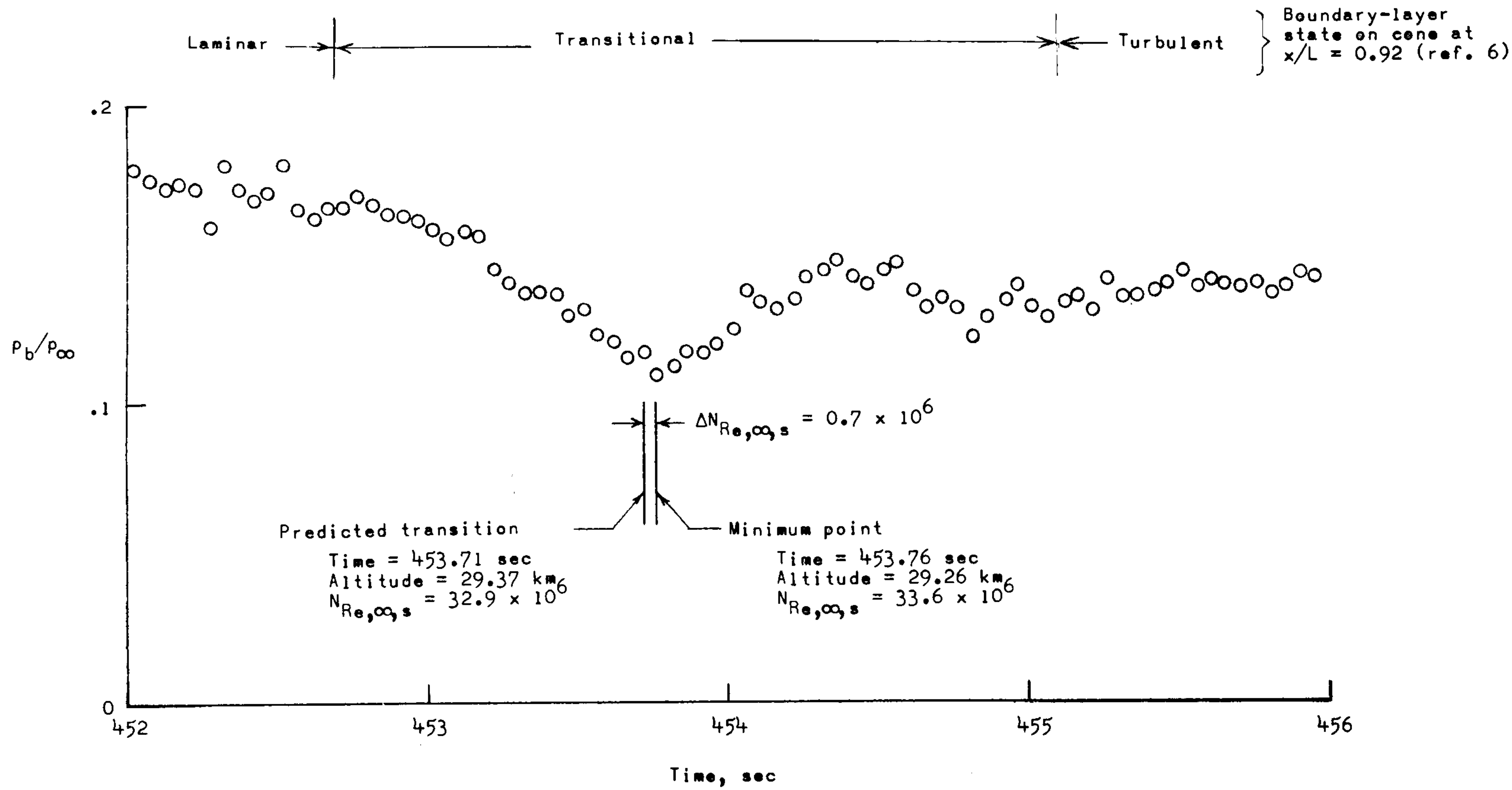

Figure 9.- Nominal transition time as indicated by center base pressure and the method of reference 10.

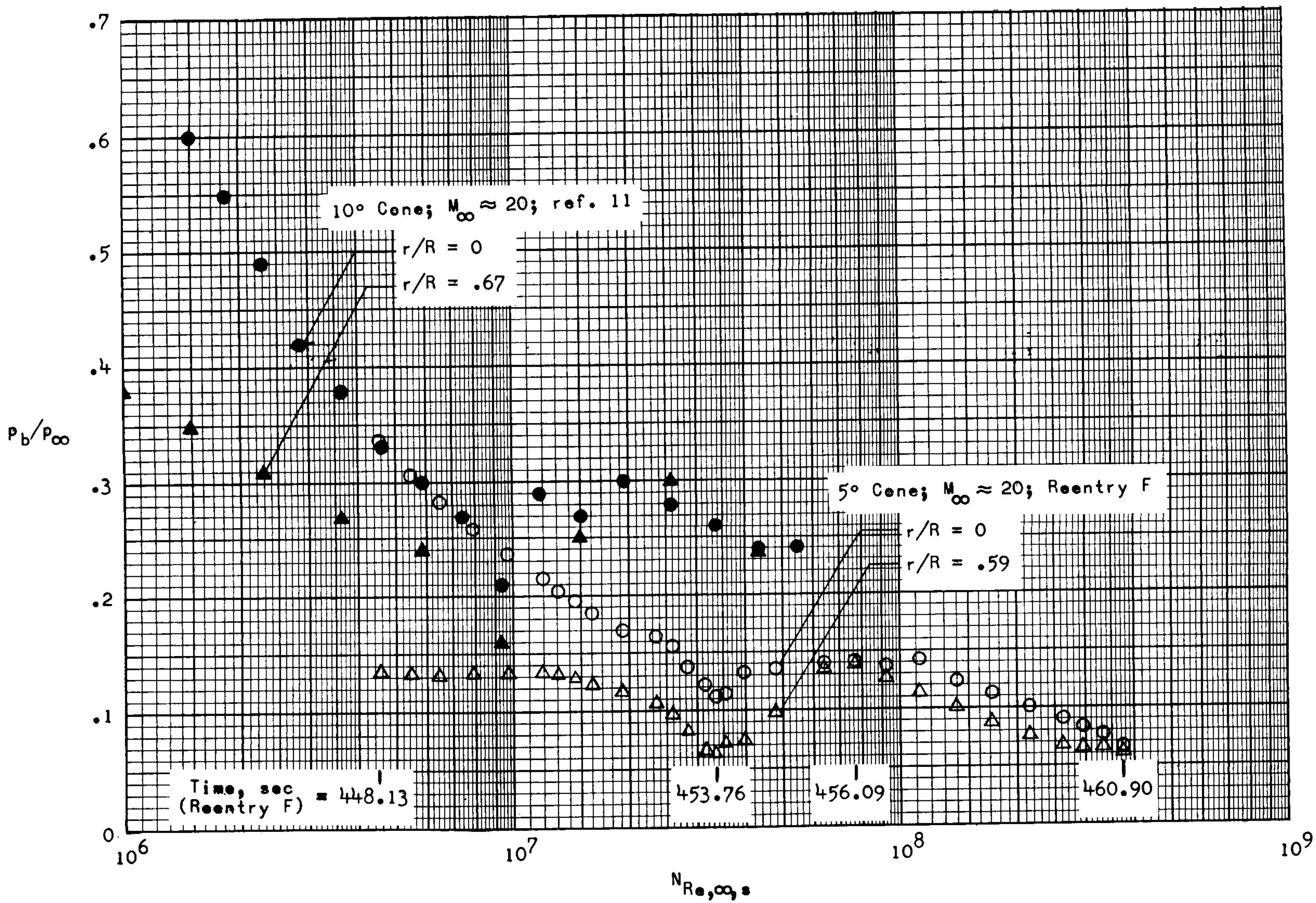

Figure 10.- Variation of base pressure with free-stream Reynolds number for two cone configurations.

[redacted]

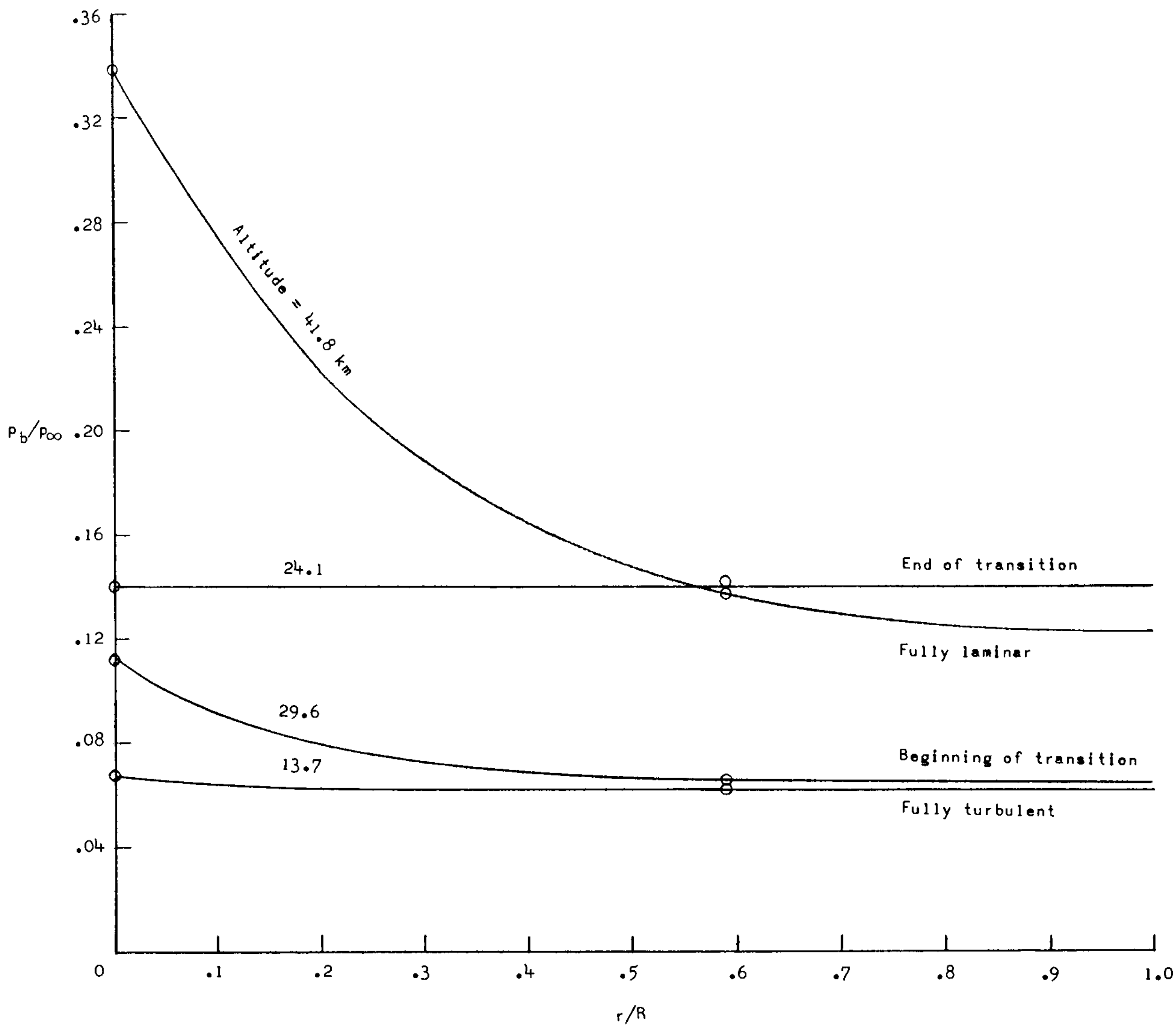

Figure 11.- Variation of pressure distribution on the base with type of boundary layer indicated by base pressure.

[redacted]

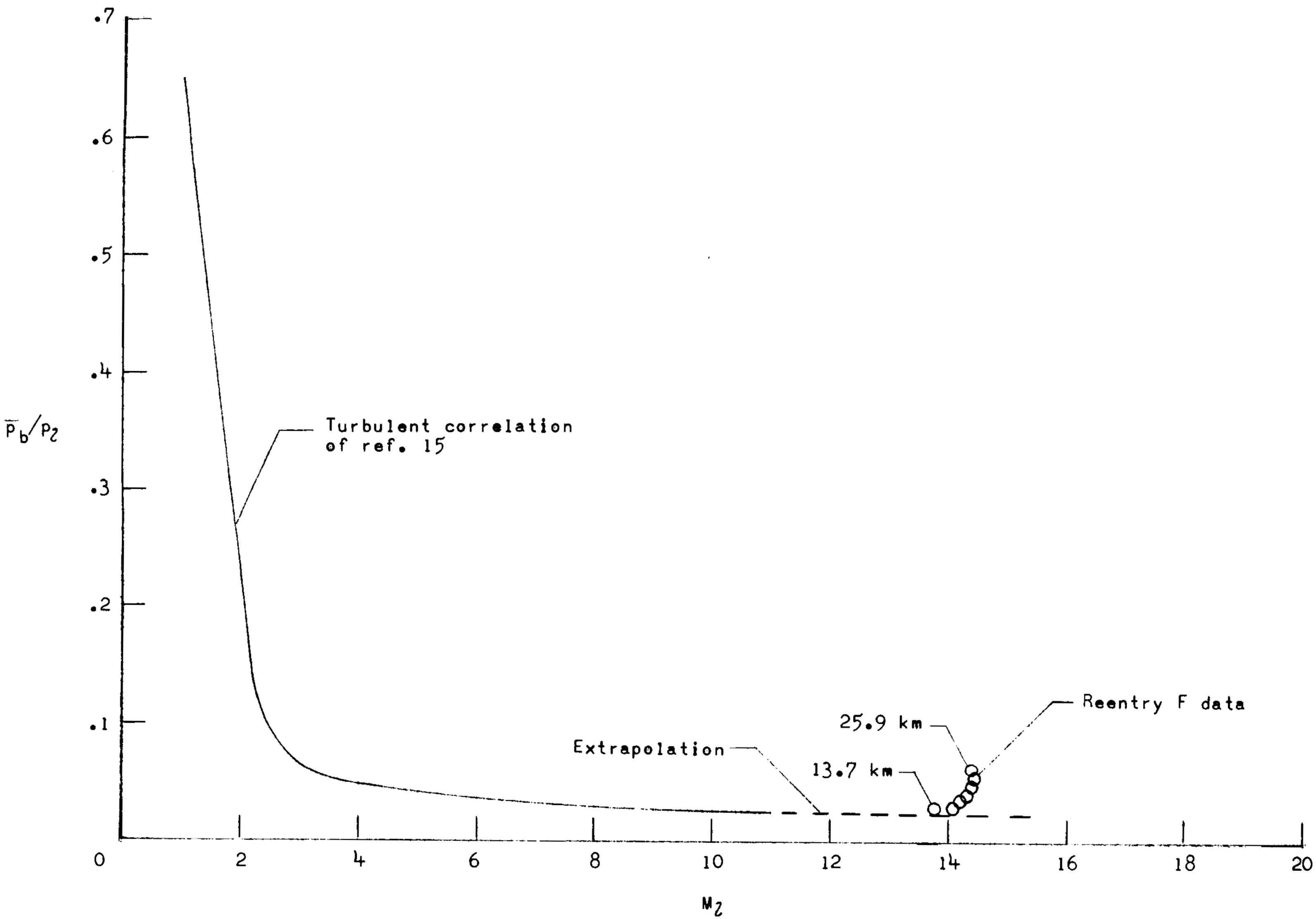

Figure 12.- Comparison of turbulent average base pressure on the Reentry F spacecraft with the turbulent correlation of reference 15.

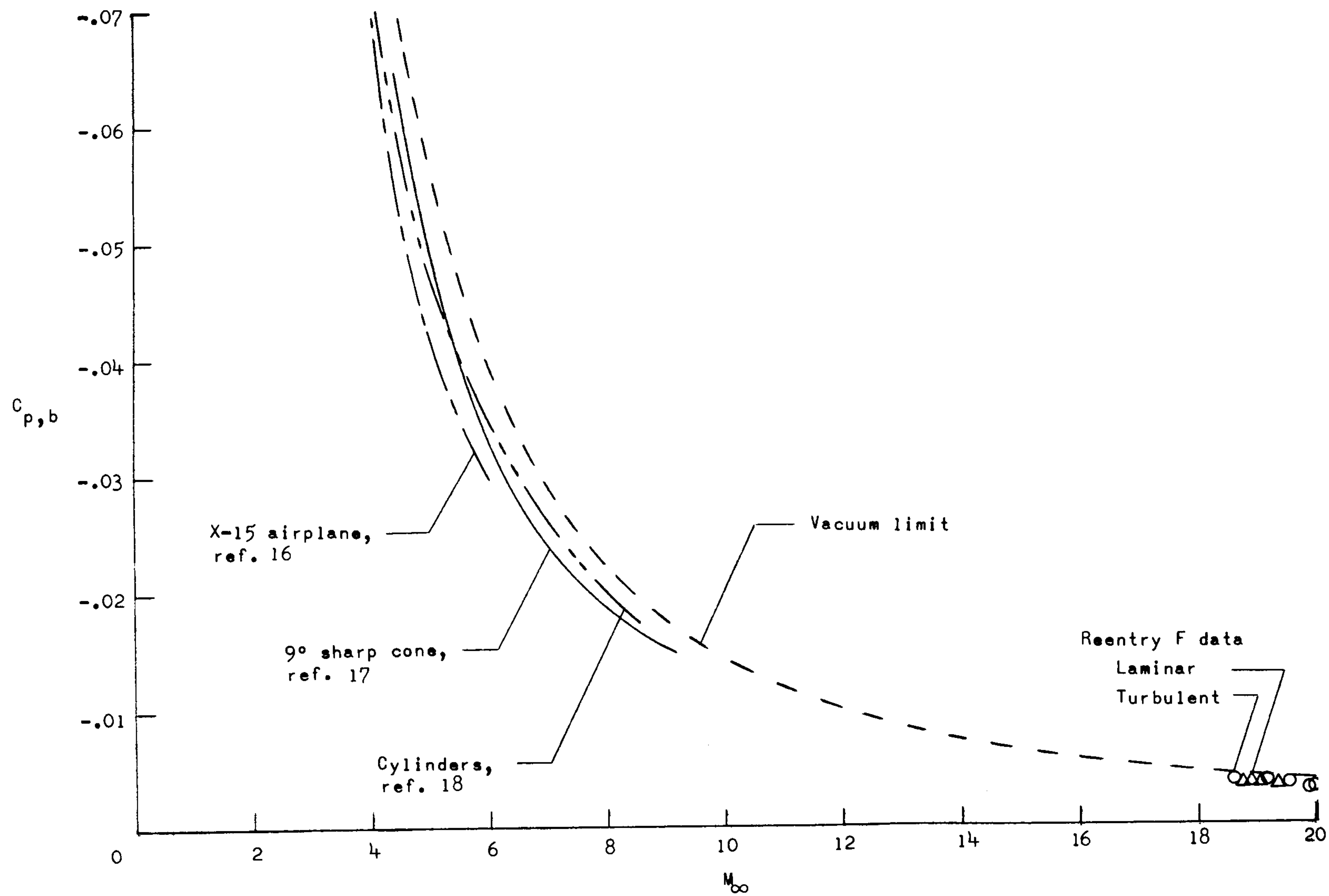

Figure 13.- Variation of base pressure coefficient with free-stream Mach number showing comparison of Reentry F and other data with vacuum limit curve.

[redacted]

[redacted]

[redacted]

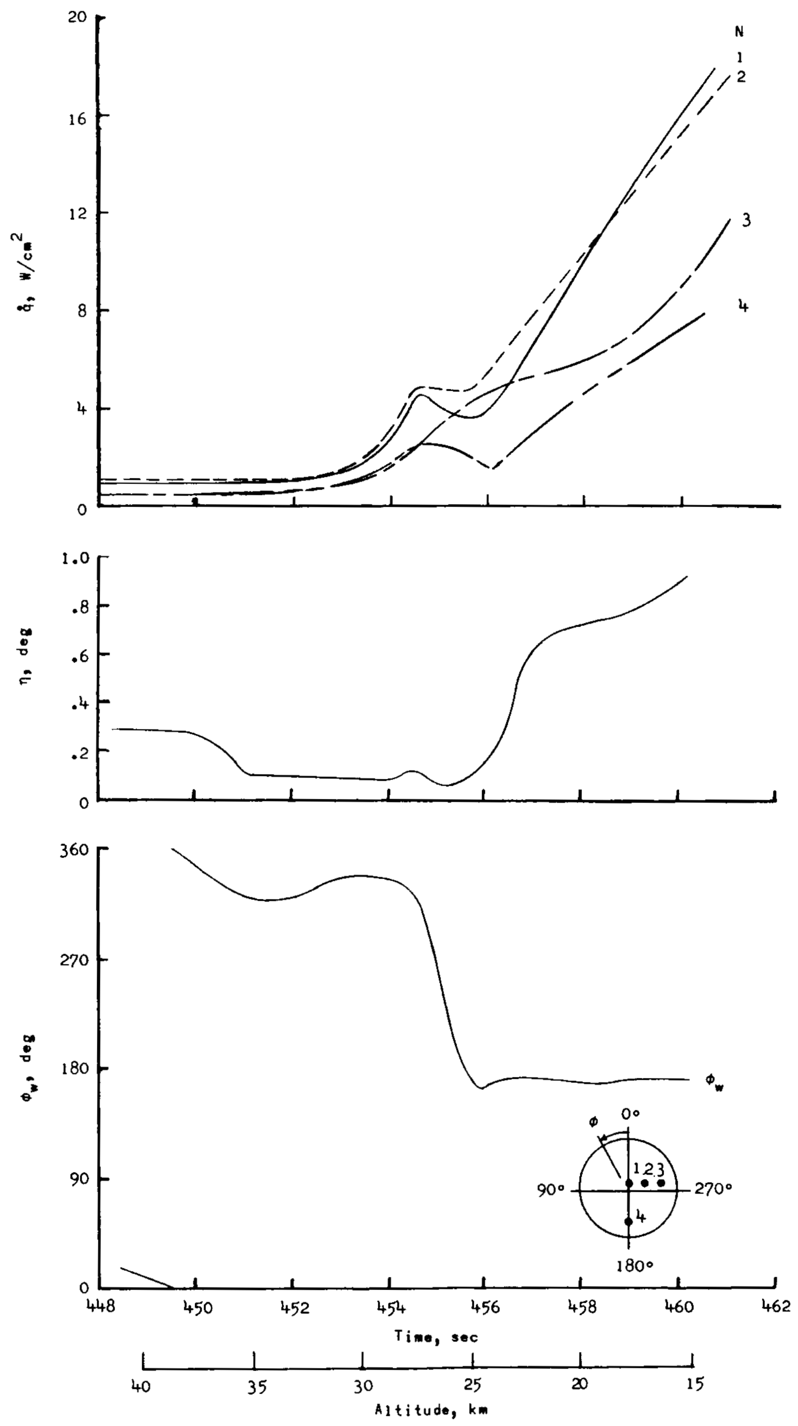

Figure 14.- Heating-rate distribution, mean total angle of attack, and spacecraft orientation time histories.

[redacted]

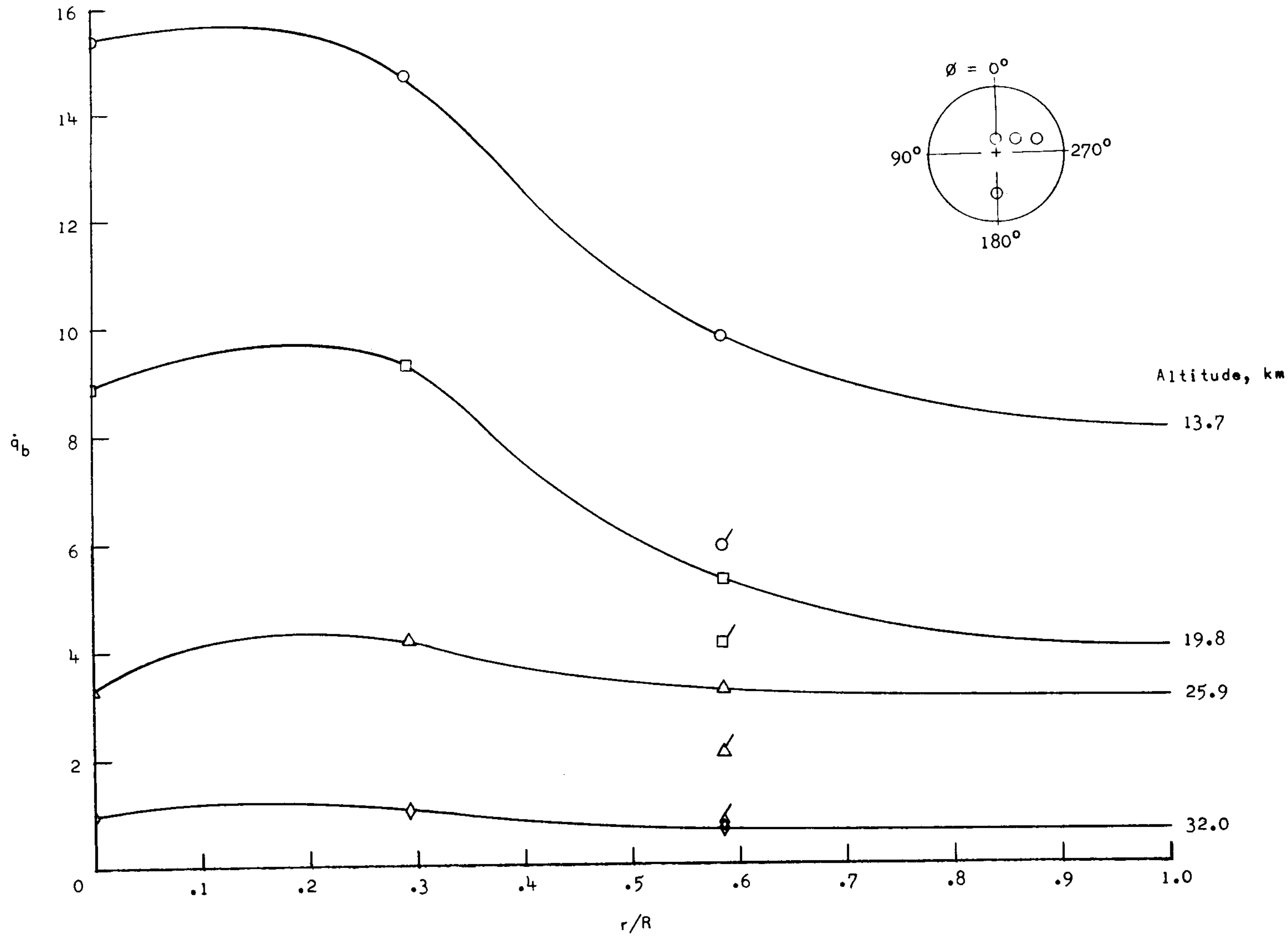

Figure 15.- Representative heating-rate distribution near one radius of the base ($\phi = 270^\circ$) during reentry. Flagged symbols represent measurements on another radius ($\phi = 180^\circ$).

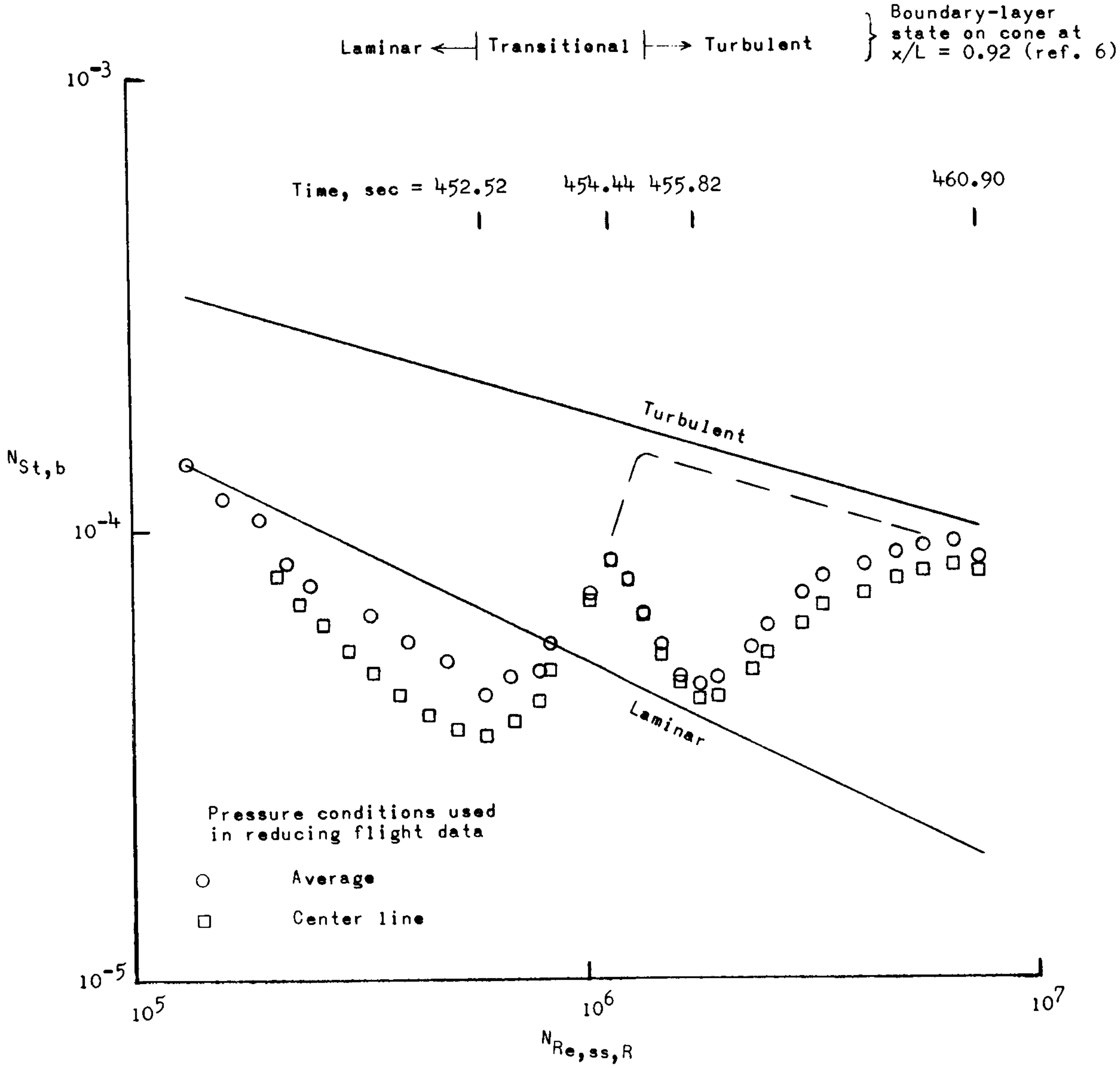

(a) Method of equations (1) and (2).

Figure 16.- Comparison of Reentry F base heating rates with two correlation methods.

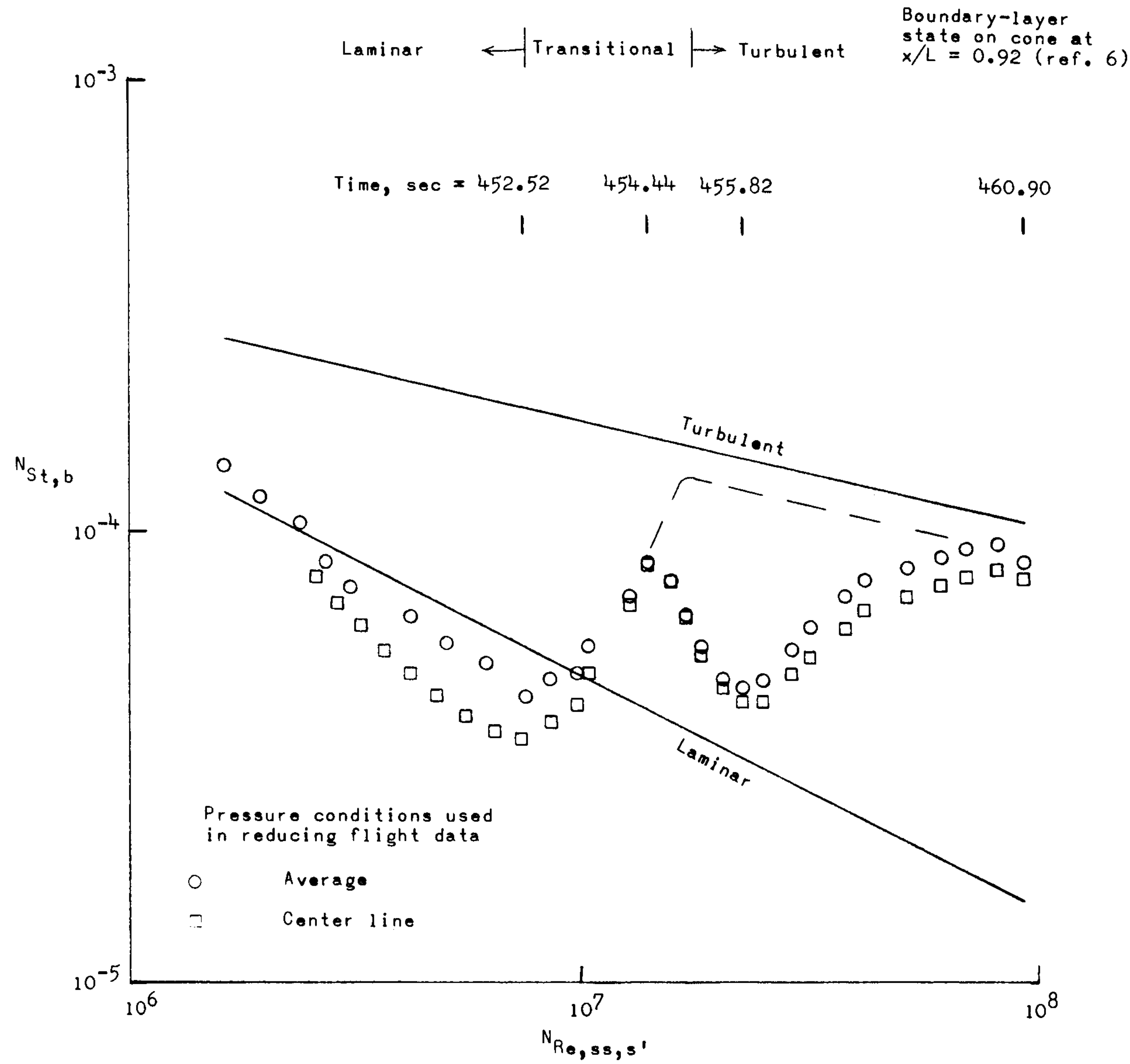

(b) Method of equations (3) and (4).

Figure 16.- Concluded.

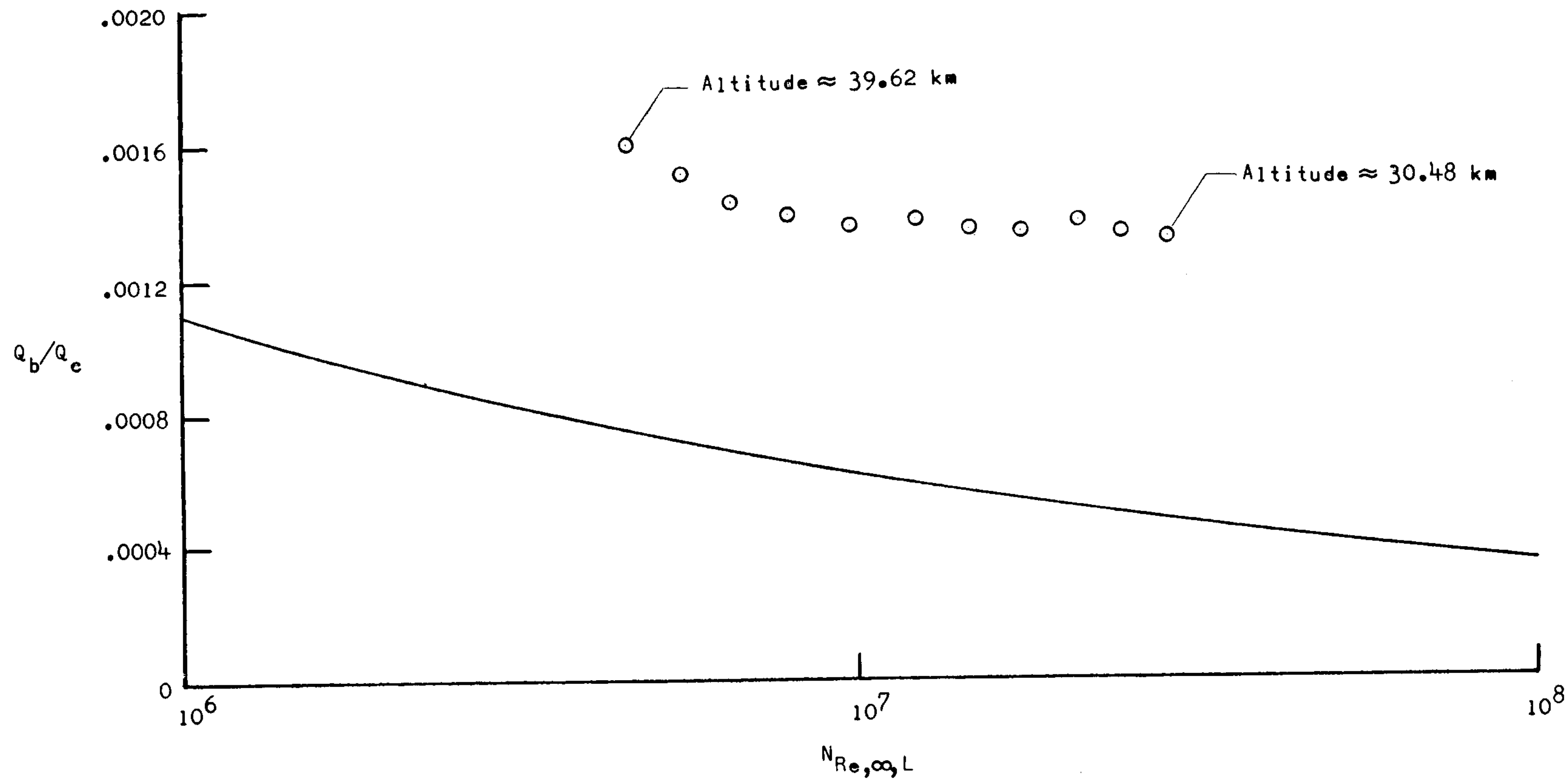

Figure 17.- Comparison of the laminar correlation method of reference 21 and the Reentry F base heating.